CR-73248

AVAILABLE TO THE PUBLIC

ME-TR-033-5

HEAT TRANSFER BETWEEN SURFACES IN CONTACT:

THE EFFECT OF LOW CONDUCTANCE INTERSTITIAL MATERIALS

PARTS IV and V

INVESTIGATION OF THERMAL ISOLATION MATERIALS AND

THEIR APPLICATION IN BOLTED FLAN

by

D.A. Gyorog and P.A. Smuda

GPO PRICE $ _____

CSFTI PRICE(S) $ _____

Hard copy (HC) 3.00

Microfiche (MF) .65

ff 653 July 65

Research Sponsored by

AMES RESEARCH CENTER

NATIONAL AERONAUTICS AND SPACE ADMINISTRATION

under Grant NGR 03-001-033

Mechanical Engineering Department
Arizona State University
Tempe, Arizona

AUGUST, 1968

HEAT TRANSFER BETWEEN SURFACES IN CONTACT:

THE EFFECT OF LOW CONDUCTANCE INTERSTITIAL MATERIALS

PARTS IV AND V

INVESTIGATION OF THERMAL ISOLATION MATERIALS AND

THEIR APPLICATION IN BOLTED FLANGE JOINTS

by

D. A. Gyorog and P. A. Smuda

Research Sponsored by
Ames Research Center

NATIONAL AERONAUTICS AND SPACE ADMINISTRATION
under Grant NGR 03-001-033

Mechanical Engineering Department
Arizona State University
Tempe, Arizona

August, 1968

ACKNOWLEDGMENTS

The authors wish to express their appreciation to the National Aeronautics and Space Administration for financial support and to Ames Research Center for the loan of the test apparatus used in this study.

Special thanks and gratitude is also expressed to Rod McIntire, Joe Smith, Frank Hombaker, Robert MacMillan, Dick Fisher and Carlton Anderson for their exceptional help in the construction of the test facility and apparatus.

Finally, special appreciation is expressed to Harold Broda for typing the manuscript.

TABLE OF CONTENTS

LIST OF TABLES

LIST OF FIGURES

NOMENCLATURE

A	Apparent area, sq ft
h	Junction thermal conductance, Btu/hr sq ft ^{o}F
I	Current, amps
k	Thermal conductivity, Btu/hr sq ft ^{o}F
L	Load, pounds
ℓ	Thickness, inches
M	Mesh size
n	Number of layers
P	Pressure, psi
Q	Heat transfer, Btu/hr
q	Heat flux, Btu/hr sq ft
R	Junction thermal resistance, hr sq ft ^{o}F/Btu
r	Resistance, ohms
T	Temperature, ^{o}F
ΔT	Junction temperature difference, ^{o}F
dt	Increment of temperature, ^{o}F
W	Weight, pounds
dx	Increment of length, inches
δ	Uncertainty increment
ρ	Density, lb/cu ft

Subscripts

o	Initial
C	Cooled
c	Per contact
e	Effective
H	Heated
ℓ	Heat loss
M	Bulk material
m	Mean

CHAPTER I

INTRODUCTION

The successful operation of a spacecraft is, to a great extent, dependent upon the temperature control of its components and surfaces. As missions become more demanding, i.e. longer lifetime, near solar missions, etc., the use of protective shields and other insulation techniques take on increased importance. For most structures the thermal analysis requires design information regarding the thermal conductance of joints. A great number of examples from current spacecraft technology can be listed for which the thermal contact conductance is an important design parameter. Some of these are the thermal isolation of components such as reflective shields, antenna struts, and cryogenic storage compartments. In these particular cases the insulating effect of low conductance interstitial materials would have a direct benefit.

Although the measurement and prediction of thermal contact resistance has received considerable attention, the results have been somewhat disappointing because of the lack of reproducible data and the difficulty of predicting joint conductance under varying conditions of manufacture, load, and surface conditions (1)*. One proposed solution to enable the prediction of thermal resistance is the use of contact filler materials which are more or less insensitive to loads and surface conditions. The insertion of interstitial materials can serve to increase or decrease the thermal resistance of the

*Numbers in parentheses refer to references.

junction. However, specific results on the thermal conductance of metallic contacts with interstitial fillers are limited. Further, design information for thermal isolation is even more limited since the majority of the previous investigations on this subject have emphasized the improvement of the contact conductance with such materials as high conductivity metal foils. Thus the primary purpose of this investigation was to provide information, based on experiment, for thermal insulation of contacts with low conductance interstitial materials.

In a vacuum environment the heat transfer at the contacting surface is a result of conduction through the interstitial material and for some materials possible radiation heat transfer. Calculations for the metal test specimen temperatures encountered during the investigation indicate that the contribution due to radiation is less than 0.1 percent. Hence the primary mode of heat transfer is conduction. The effective thermal resistance at the junction can therefore be increased by use of a low thermal conductivity material and by reduction of the contact area. Junction materials which provide the desired increase in thermal resistance can be classified into the following general categories: Geometric, Powders, and Insulation Sheets. The thermal contact conductance of the junction is defined as

$$h = \frac{Q}{A(T_1 - T_2)}$$

where T_1 and T_2 are the extrapolated temperatures of the bounding surfaces of the contact and Q/A is the apparent heat flux of the total cross-sectional area of the contact. Thus the thermal contact resistance, R, is defined as the reciprocal of the product hA.

The investigation was composed of five distinct parts:

Part I - Assembly and experimental verification of the test apparatus,

Part II - Comparative study of interstitial materials,

Part III - Detailed study of promising materials,

Part IV - Study of other promising materials and combinations of materials for multilayer interstitial configurations, and

Part V - Application to flange joints used in spacecraft construction.

Parts I, II and III were supported by the initial research grant and the results have been previously reported (1, 2, 3). The purpose of this report is to summarize the pertinent results of the previous phases of the investigation and to report the results of Parts IV and V.

CHAPTER II

SUMMARY OF PREVIOUS RESULTS

PART I - Experimental Verification of Test Apparatus

The primary objective of the first phase of the investigation was to assemble and test the experimental apparatus in the vacuum facility. The test apparatus had been designed and constructed at the Ames Research Center and was loaned for this investigation. In an earlier study (4) the vacuum facility and instrumentation techniques had been developed. After assembly of the test apparatus, the initial runs were conducted with armco iron specimens to check the instrumentation, to calculate the magnitude of the heat loss, to test the deviation from one-dimensional heat transfer, and to develop an experimental procedure. Following these runs, aluminum 2024 specimens were installed and the resulting thermal contact conductance values compared with those of previous investigators. As a result of these tests the apparatus was modified to include additional thermocouples, insulation, and radiation shields. Techniques were also established for specimen surface preparation, thermocouple installation, specimen alignment and loading, and general test procedures.

The design criteria and specific details of the experimental apparatus are discussed in the Part I report (1). However, schematic diagrams of the test apparatus are repeated in Figures 1 and 2 for easy reference. The test section was a one inch diameter column with the contact surface at approximately mid-height. Each metal test specimen was

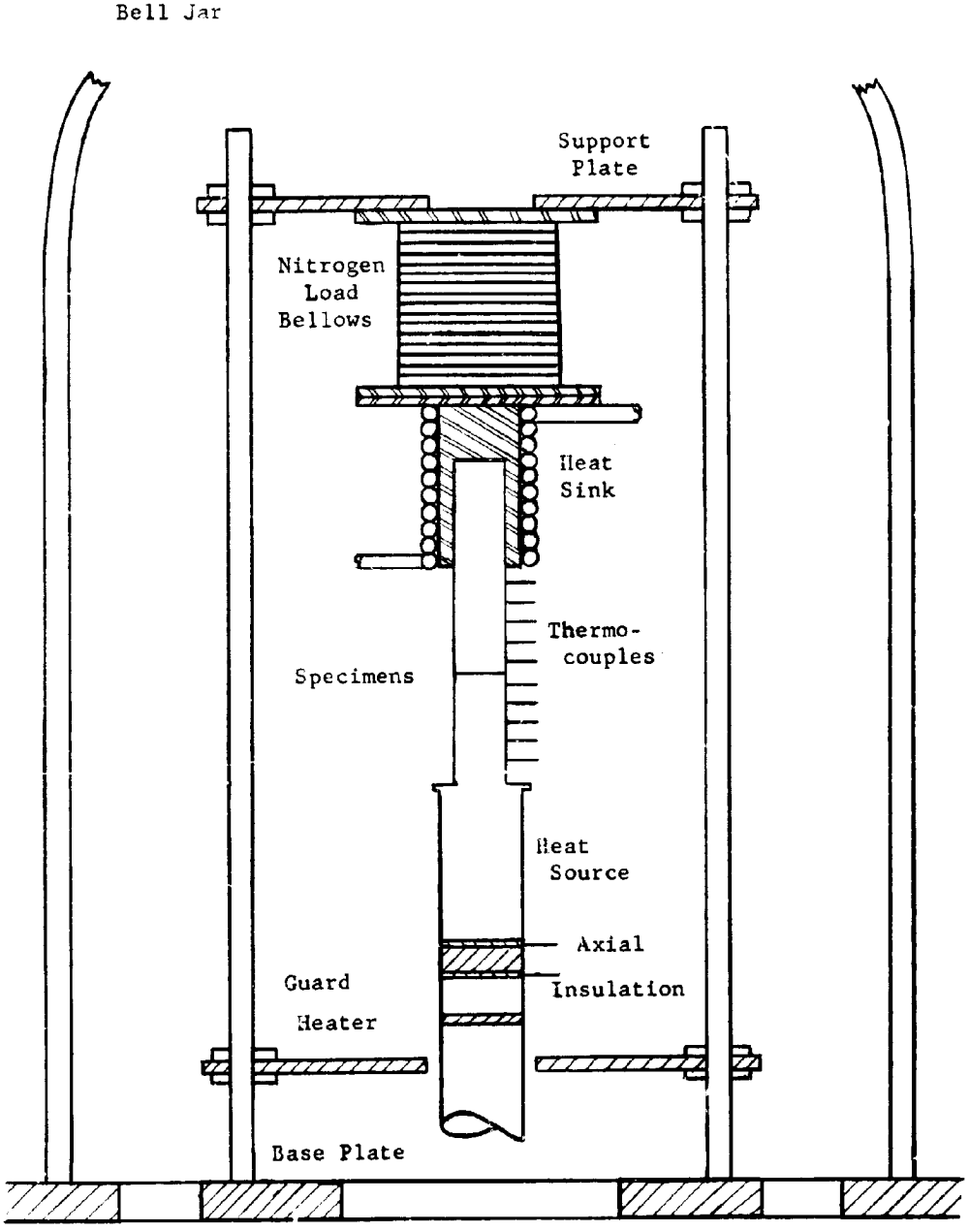

Figure 1. Schematic Diagram of the NASA Experimental Apparatus.

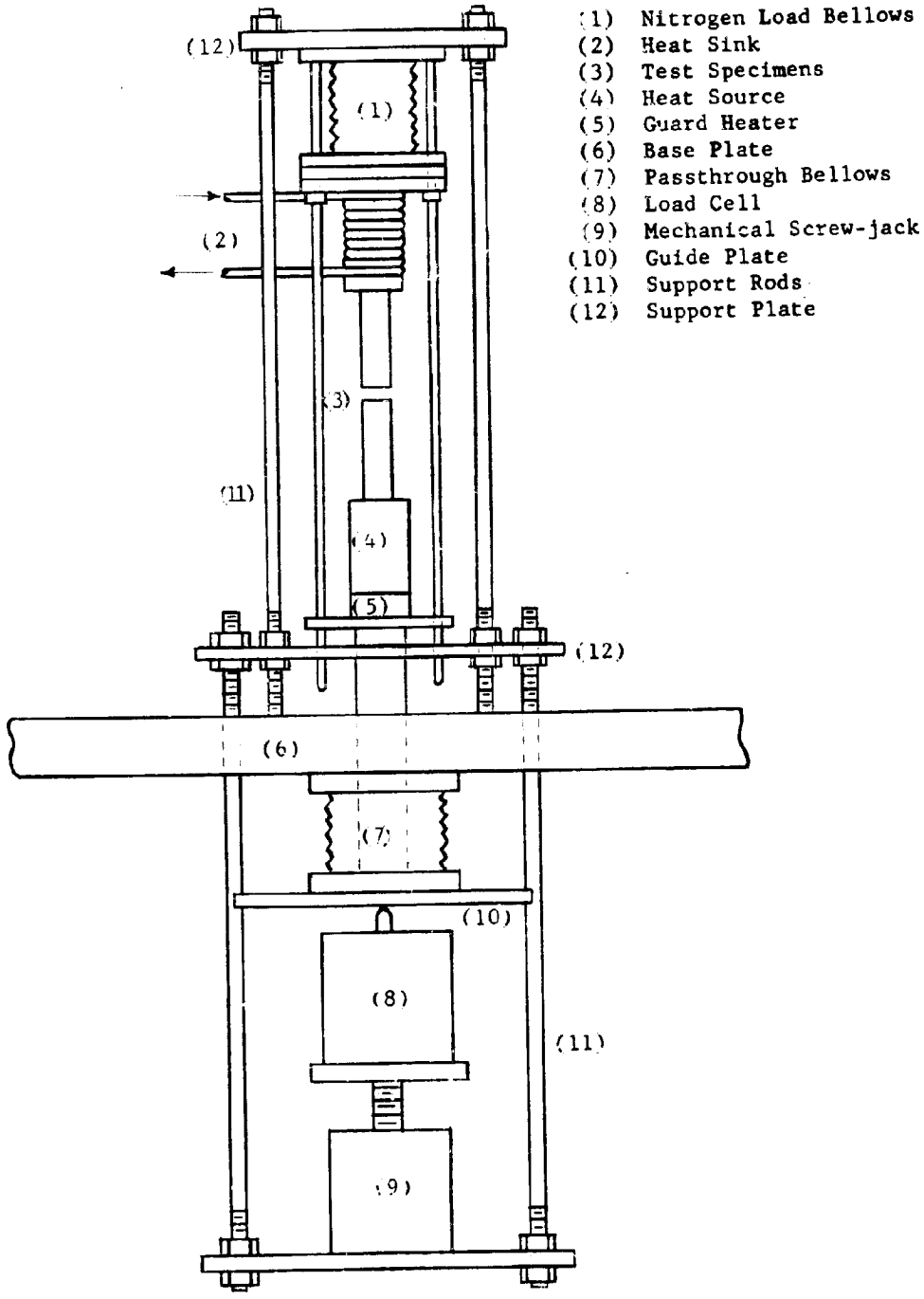

Figure 2. Diagram of the Axial Loading System.

instrumented with five centerline and three surface thermocouples. The centerline thermocouples were one-half inch apart starting one-quarter inch from the junction. These temperatures were used to calculate the temperature gradient and resulting heat flux and, in addition, the temperature at the junction was found by extrapolation. Copper-constantan 30 gage wire thermocouples were inserted into holes drilled with a No. 56 drill and carefully packed in place with aluminum powder. The first two specimen sets were x-rayed to check the thermocouple installation and determine drill runout. Since no flaws were detected it was deemed unnecessary to continue this procedure for all specimens. The continuity of the thermocouples was also checked before and after installation. Surface thermocouples were placed in one-sixteenth inch deep holes diametrically opposite the centerline thermocouple. Thermocouple leads were wrapped around the specimen to reduce the heat transfer from the junction. The thermocouples, lead wires and thermocouple switches were calibrated with reference to a Platinum-Platinum 10% Rhodium thermocouple and an uncertainty of 0.5% was established.

For load application to the test specimens, high pressure nitrogen gas was admitted to the stainless steel bellows chamber (Fig. 2). The nitrogen bellows was selected since it simplified specimen loading and provided a relatively accurate means of adjusting and maintaining a constant load. The load pressure, P, is defined as the load force divided by the cross-sectional area of the cylindrical test specimen. A calibrated load cell and strain indicator were used to measure the load force. These measurements were corrected for the deflection of the stainless steel load pass-through bellows and the atmospheric pressure differential.

Since the thermal conductivity of the metal test specimen is essential to the calculation of the heat flux, it was desirable to establish that published values for k were applicable to the test specimen material. An apparatus consisting of a central heater sandwiched between two 4-inch long by 1-5/8 inch diameter cylinders of the test material was constructed. Each end of the column was attached to a liquid cooled plate and heater combination which was adjusted to maintain a given temperature difference. Temperature gradients were calculated from measurements obtained by thermocouples imbedded in the material. Armco iron specimens were installed to calibrate the apparatus for heat loss since the k values for armco iron are relatively well established (5). Then thermal conductivity values for the test specimen materials were determined. These values agreed within 5 percent of the published data so for all subsequent calculations the thermal conductivity values were obtained from References 6, 7, and 8.

A band heater was clamped around the end of the heated test specimen (Fig. 1). This portion of the test specimen was insulated and surrounded by a radiation shield to reduce the heat transferred to the adjacent apparatus. Aluminum foil radiation shields were also installed around the thermocouple instrumented portions of the heated and cooled test specimens. Because a large temperature difference (200°F to 400°F) existed between the two specimens, with the interstitial materials in place, the radiation shields were separated at the contact plane. Chilled water and liquid nitrogen coolant fluids were supplied to the copper heat sinks.

The bare junction experimental results for aluminum 2024 were shown to indicate the same trends and relative magnitudes as those of other investigators. Thermal contact conductance values for repeat test runs agreed within 5 percent. The uncertainties in the calculated values of h were estimated to vary from 7.2 percent at lower values of h to 11.6 percent at higher values. This variation is a result of the reduction in junction temperature difference with increasing h.

PART II - Comparative Study of Interstitial Materials

During this phase of the investigation thermal tests in a vacuum environment of 10^{-5} Torr were conducted to experimentally ascertain which were the most promising junction insulation materials. A list of possible materials was first compiled from a survey of the materials literature and from correspondence with industrial concerns. In order to effectively accomplish the experimental study within the required time the number and types of materials were restricted to those listed in Table 1. The results of these comparison runs were reported in Reference 2 and 3.

Since the purpose was to increase the resistance to heat transfer at a junction, smooth test surfaces were selected since they provide the minimum resistance for bare junction conditions. To minimize deviations in contact resistance between different sets of test specimens, the same surface finishing technique was followed for all specimens. The contacting surfaces were finished on a lathe and then lapped and polished. Measurements with a profilometer and proficorder

TABLE 1

MANUFACTURER'S PROPERTY DATA

MATERIAL	RUN SYMBOL	SUPPLIER	K Btu/hr.ft°F	ρ lb_m/ft^3	VACUUM WEIGHT / AIR WEIGHT	ℓ_o in
Asbestos Board	AB	Johns-Manville	0.04 - 100°F 0.06 - 500°F	136	---	0.1210
Asbestos Tape (No. 2074)	AT	Atlas Asbestos Company	0.12 - 300°F	55	0.985	0.0810
Carbon Paper F-907	CA	Fiberite Corp.	0.2 - 300°F	9	0.993	0.0550
Ceramic Paper 970-J	CE	Carborundum Company	0.03 - 400°F 0.10 -1600°F	12	0.999	0.1080
WRP-X-AQ Felt	FE	Refractory Products Co.	0.04 - 500°F 0.12 -2000°F	18	0.995	0.1830
Laminate T-30LR	LA	Carborundum Company	0.37 - 250°F 0.13 -2000°F	50	0.989	0.1240
Magnesia 25	MA	Degussa Inc.	15.7 - 112°F	196	---	0.0990
Mica (Bonded)	MI	Regan Engineering	.21 - 100°F 1.24 -1000°F	13	0.999	0.0034
Pluton B-1 Cloth	PL	3M Company	0.02 - 80°F 0.03 - 180°F	87	---	0.0270
Pyroid	PY	Pyrogenics I c.	1.00 - 70°F 0.30 -5000°F	162	---	0.1156
Pyrotex 23RPD	PI	Raybestos-Manhattan	1.39 - 70°F	---	---	0.1120

TABLE 1 (Cont'd.)

MATERIAL	RUN SYMBOL	SUPPLIER	K Btu/hr.ft°F	ρ lb_m/ft^3	VACUUM WEIGHT / AIR WEIGHT	ℓ_o in
Silica Paper F-904	SI	Fiberite Corp.	0.10 - 300°F	10	0.992	0.0495
S.S. Screen 10/in	SS 10	---	9.30 - 212°F	500	---	0.0500
S.S. Screen 100/in	SS 100	---	9.30 - 212°F	500	---	0.0090
S.S. Shim	SH	---	9.30 - 212°F	500	---	0.0010
Teflon Sheet	TE	DuPont Co.	1.35 - 100°F	10	---	0.0028
Teflon TFE	TFE	Bel-Art Products	--- ---	---	---	0.062
Textolite	TX	General Electric Co.	1.40 - 250°F	---	---	0.0621
Titanium Screen 10/in	TI 10	Newark Wire Cloth Company	11.6 - 200°F	276	---	0.0500
Tungsten Screen 20/in	W20	Newark Wire Cloth Company	96 - 32°F 70 - 932°F	1210	---	0.0140
Zirconia 23	ZI	Degussa Inc.	1.08 - 212°F	355	---	0.1048

indicated a 3 to 6 μ-inch roughness and approximately a 20 to 25 μ-inch flatness deviation. The similarity of the surfaces was substantiated by the agreement of the bare junction conductance values for the different specimen sets. So that the comparison of the different materials would be independent of temperature two mean temperatures were selected for all of the tests, +190°F and -100°F. For the higher temperature runs the heated specimen was maintained at 300°F by adjusting the heater power input and the flowrate of cooling water which was at a temperature of approximately 60°F. To attain the lower temperatures liquid nitrogen was used as the coolant which produced temperatures as low as -300°F in the low temperature specimen. The heated specimen was adjusted to approximately 90°F for these runs.

Generally from six to eight hours were required to attain a steady-state condition. The experimental runs with bare junctions and with interstitial materials were conducted in the order of increasing load pressure. In all tests one specimen was at a more extreme temperature, +300°F or -300°F, while the other was nearer the ambient temperature. Since the temperature measurement error should be less and the assumption of one-dimensional heat flow better for the ambient temperature specimen, the heat flux calculated for this specimen was used to calculate h. However, some uncertainty exists in the selection of the "best" temperature gradient especially for small heat flux values (low h). For this reason maximum and minimum slopes were estimated which usually gave a difference of from 2 to 3 Btu/hr ft^2 °F between the high and low values of h for thermal conductance values less than 10 Btu/hr ft^2 °F. This increased to a difference between the

high and low values of h of 20 Btu/hr ft^2 ^oF at thermal conductance values near 400 Btu/hr ft^2 ^oF. The increased deviation results as a consequence of the reduction in the junction temperature difference. To provide a better estimate of the contact conductance for the low heat flux cases, the heat flux was also calculated by determining the energy losses from the heated specimen in Part III. The results of the comparative study (190^oF mean temperature) are graphically illustrated in Fig. 3. The initial thicknesses of the test materials are listed in Table 1. Only the eight materials having the lowest thermal contact conductances in the high temperature tests (Fig. 3) were considered in the low temperature comparison tests (2). The thermal contact conductance decreased from 10 to 50 percent for these materials with the reduction in the mean temperature from $+190^oF$ to -100^oF. This reduction can be attributed to changes in material properties with temperature.

The initial series of bare junction tests were conducted with specimen set 1, which was machined from "as received" aluminum stock. A description of the different test specimens is given in Table 2. The resulting bare junction conductance values for the test specimens is illustrated in Fig. 4. Initially the ratio of calculated temperature gradients in the heated and cooled specimens for set 1 was 1.28, nearly equal to the ratio of thermal conductivity of 1.2 for "as received" aluminum. However, after heating set 1 to high temperatures it was found that the temperature gradient ratio increased to 1.4, which compares to the thermal conductivity ratio of "annealed" aluminum in the heated specimen and "as received" aluminum in the cooled specimen. This property

TABLE 2

METAL SPECIMEN DESIGNATION

SPECIMEN NO.	MATERIAL TYPE		SURFACE CONDITIONS	
	Hot Specimen	Cold Specimen	Hot Specimen	Cold Specimen
1	Aluminum 2024 AN	Aluminum 2024 UN	A	A
2	Aluminum 2024 AN	Aluminum 2024 AN	A	A
3	Aluminum 2024 AN	Aluminum 2024 AN	A	A
4	Aluminum 2024 AN	Aluminum 2024 AN	A	A
5	Aluminum 2024 AN	Aluminum 2024 AN	A	B
6	Stainless Steel 304	Stainless Steel 304	A	A
7	Stainless Steel 304	Stainless Steel 304	A	A

Notation

AN - Specimens annealed at 600°F for 24 hrs.

UN - Specimen unannealed

A - Roughness 3-5 μin Flatness 20-25 μin

B - Roughness 200-225 μin Flatness 25-50 μin

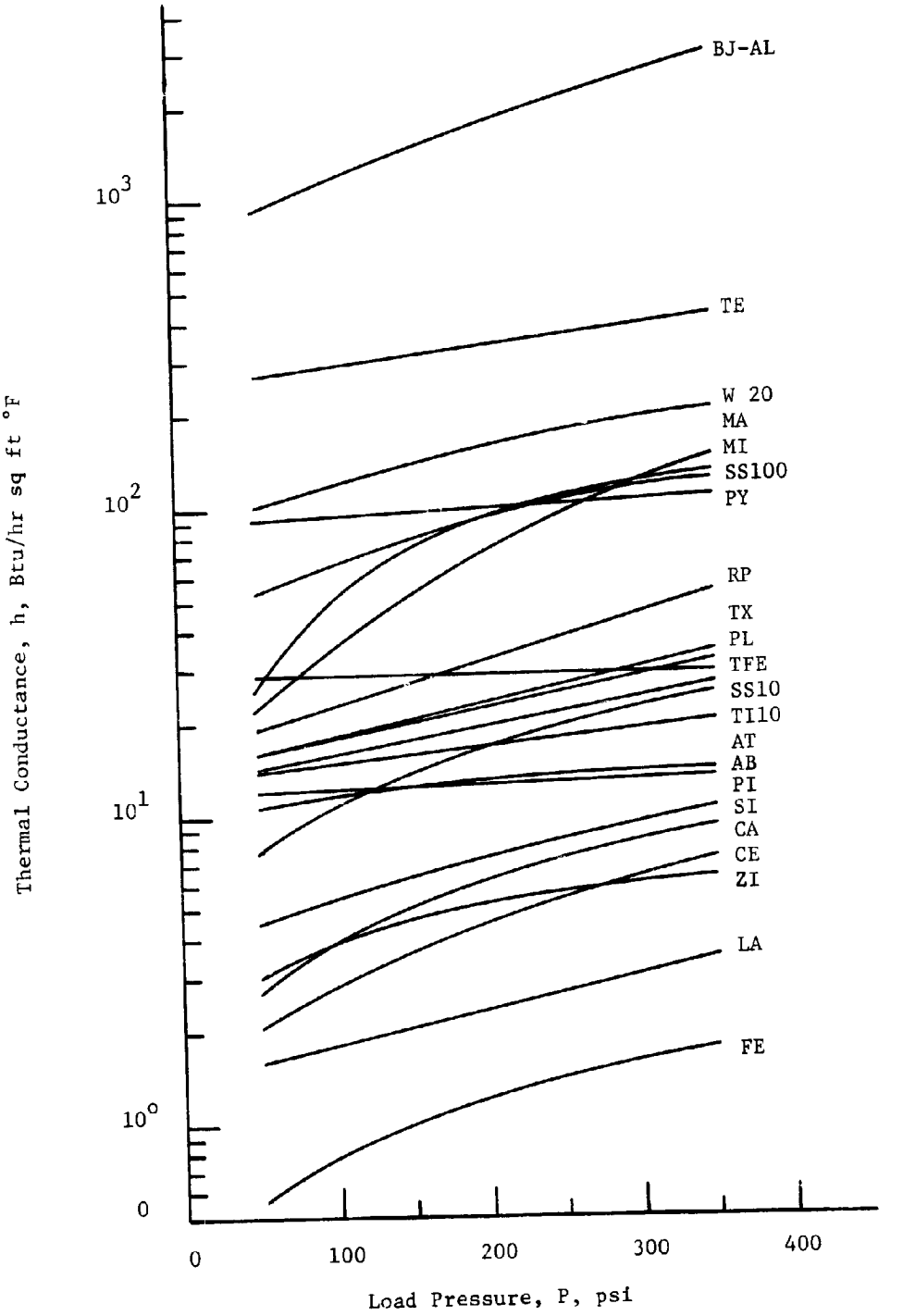

FIGURE 3. Comparative Plot of Thermal Contact Conductance

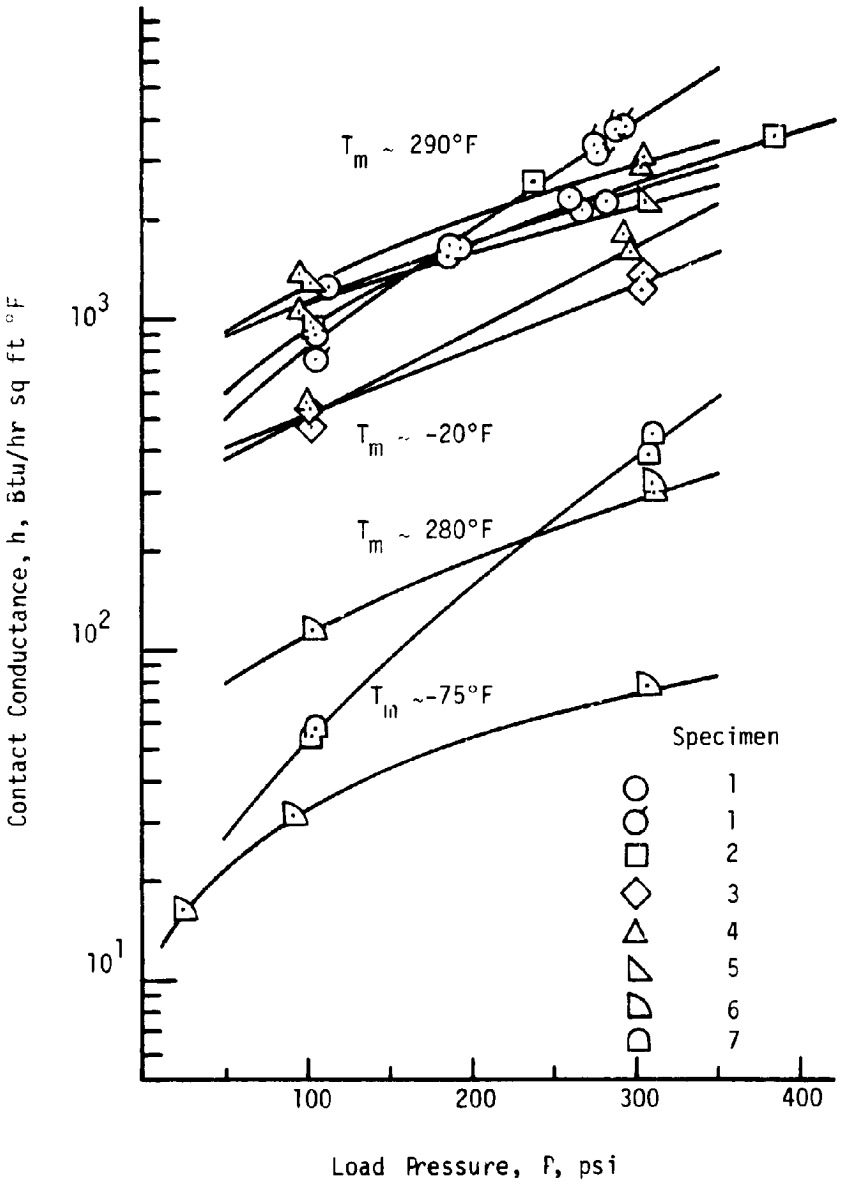

FIGURE 4. Thermal Contact Conductance of Bare Junctions

variation, which must be attributed to a slow annealing of the heated specimen while subjected to a compressive load, caused a definite change in the bare junction h values. These are denoted in Fig. 4 by the flagged symbols. Thus the heated specimen of set 1 was treated as "annealed" and the cooled psecimen as "as received". Since the heat transferred was calculated by the temperature gradients in the cooled specimen, the h values for interstitial materials obtained with set 1 were not affected. This was confirmed in Part III by repeat runs with other metal test specimens. To assume that property changes would not occur in future runs, beginning with set 2 all aluminum specimens were annealed by heating in an oven to 600°F for 24 hours prior to finishing the specimen surfaces. Subsequent comparisons of the temperature gradient and thermal conductivity ratios for the annealed specimens showed excellent agreement and did not indicate any further property variation.

Many bare junction runs were interspersed between the interstitial material runs to test for changes in the surface conditions. In some cases large variations in h were encountered, but these were generally found to be the result of some surface effect such as oxidation, contamination by the previous material, or a scratch or imperfection. Only initial test runs with each specimen set (i.e. before interstitial material runs) or runs after cleaning the contact surfaces are plotted in Fig. 4 to establish a curve to compare interstitial materials. To limit the degree of oxidation the test specimens were allowed to cool in the vacuum chamber after a test. Then nitrogen gas was released into the bell jar to aid in the final cooling.

Although the laminate type T-30LR and the WRP-X-AQ felt seem to provide the best thermal insulation characteristics, the effect of the insulation thickness must also be considered. As a result, further tests with the fibre papers and mica were conducted in Part III. However, the surface of the silica paper in contact with the 300°F surface discolored as if scorched due possibly to a bonding deterioration.

PART III - Detailed Study of Promising Materials

The experimental procedure was essentially the same for all tests. First the metal test specimens were installed and tested in a bare junction configuration and then a one-inch diameter disk of the interstitial material was positioned between the metal specimens. The alignment of the test column during the evacuation of the test chamber was maintained by a slight contact pressure. After setting the test conditions the guard heater (Fig. 1) was monitored and adjusted to maintain a temperature difference of less than 5°F across the axial insulator. The results for these tests were reported in References 2 and 3.

As noted in Part II, the initial thicknesses of the different interstitial materials were not the same and because the thickness, ℓ, varies with the load pressure, the comparison of junction thermal resistance, R, for the different materials should account for the material thickness. A better comparison would be the thermal resistance per unit thickness, R/ℓ. To obtain the necessary thickness information, compression tests were run with material samples similar to those used for the thermal tests. The apparatus consisted of a compression testing machine and two one-inch diameter

aluminum rods with an attached extensometer. No deflection was observed in the apparatus itself in an initial run to 1000 pounds. For the interstitial materials the load was applied slowly and continuously up to 300 pounds with dial indicator readings recorded at designated increments. The effective compressive strain $(\ell_o - \ell)/\ell_o$ for the interstitial materials is illustrated in Fig. 5. Since the compressive strain may be influenced by the initial thickness for some materials, compression data were obtained for multilayer samples of carbon paper and mica. These particular materials were selected for test since the carbon paper was extremely compressible and Fry (9) in an earlier work had observed that the contact resistance for mica was a result of a surface effect. One, three and six layers of carbon paper were tested. The compression strain curves (Fig. 5) agreed within four percent of one another. On the other hand, for mica in which one, three, and five layers were run, the compressive strain curves were decidedly different. It was observed that the compressive strain for the multilayers was less than a single layer by the approximate fractional relation of one over the number of layers. The compression curves could be explained as a surface effect which would agree with Fry's conclusion. Therefore, in the opposite case, the carbon paper and materials of the same type should evidence a thermal resistance as a result of the effective thermal conductivity of the material and not a surface contact resistance.

The difficulty in discerning the temperature gradient for the metal test specimen became extremely important in the calculation of Q when the temperature gradient was on the order of $1^{\circ}F$ per inch. An uncertainty in the calculated values was

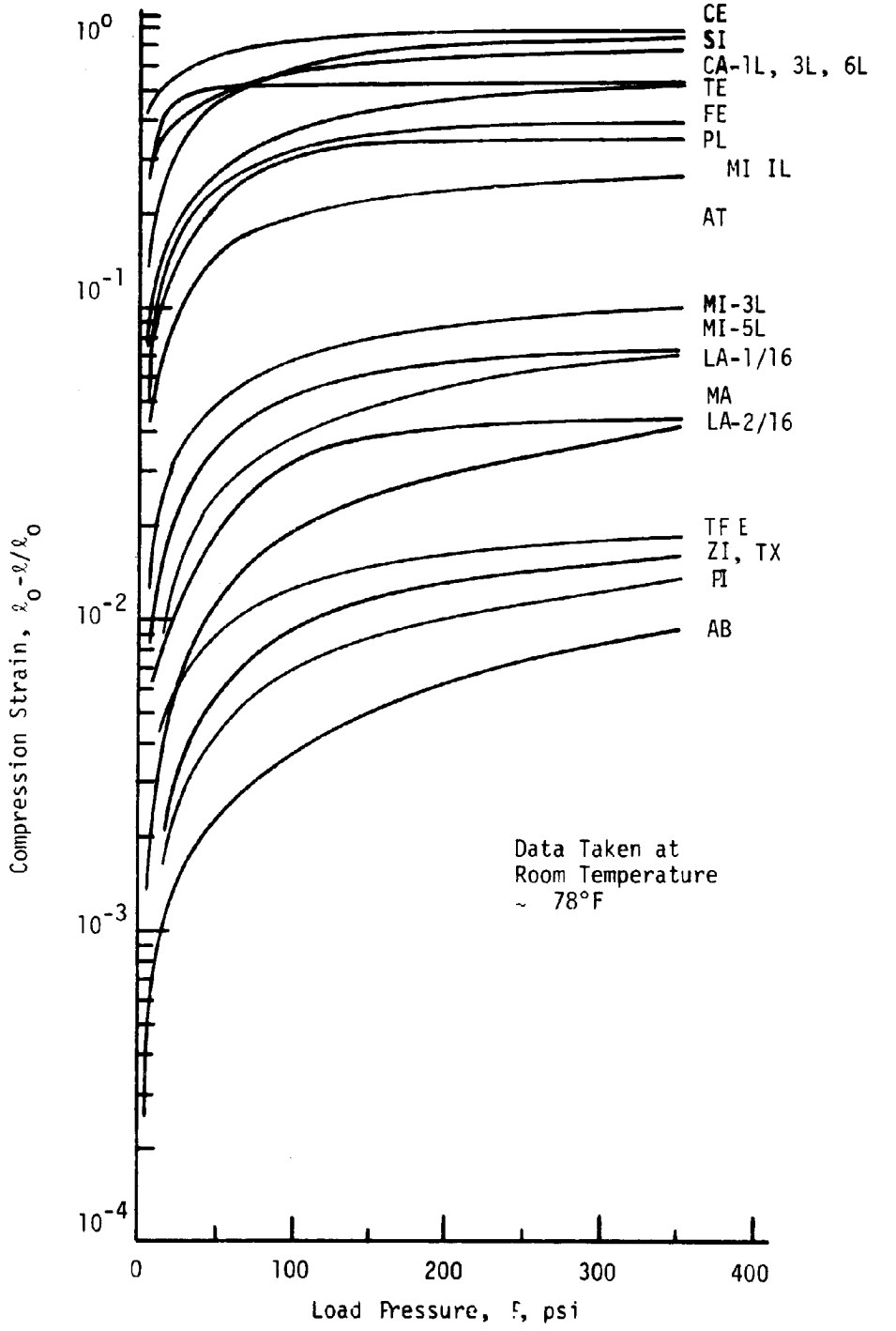

FIGURE 5. Compression Strain Curves

derived by selecting maximum and minimum temperature slopes. To improve the technique for the low heat flux cases the heat transfer at the junction was also calculated from an energy balance on the heated specimens. The energy loss calibration was essentially the same whether liquid nitrogen or water was the coolant. The differences being the temperatures of the specimens. Power input to the heater was measured at several different heater surface temperatures (comparable to those encountered in the test runs) with the test specimen contact surfaces separated slightly in the vacuum environment. Coolant flow was maintained to obtain shield and specimen temperatures close to the test values. A regulated filtered d.c. power supply was installed for the heater and the voltage and current were measured with a potentiometer and shunt arrangement. The emissivity of the specimen surfaces was estimated as 0.2. With the shield and specimen temperatures, the heat transferred by radiation from the instrumented section of the specimen to the radiation shield and from one specimen to the other across the contact gap was estimated. Subtracting these losses, an estimated loss for the thermocouple leads, and a heater lead wire resistance loss from the power input gave the energy transferred from the heater region by radiation. For the calibration runs the guard heater was monitored closely to maintain a temperature difference across the axial insulator (Fig. 1) of less than $3^{\circ}F$. Division of the resulting heat loss, Q_{ℓ}, by the temperature to the fourth power difference between the heater surface and shield yielded a radiation heat loss coefficient for the heater section. Thus for the low heat

flux runs the heat transferred at the junction

$$Q = Q_{input} - I^2r - Q_{\ell} - \left[\begin{matrix}\text{specimen surface radiation} \\ \text{loss and thermocouple loss}\end{matrix}\right]$$

The uncertainty in the energy loss calculation of Q was estimated to be from 0 2 to 0.3 Btu/hr. For an assumed uncertainty in the temperature slope of 0.5°F per inch, the approximate uncertainties in the heat transfer calculated by the product of thermal conductivity and temperature gradient are:

annealed aluminum	3 Btu/hr
as received aluminum	2 Btu/hr
stainless steel	0.3 Btu/hr

These values were estimated for the ambient temperature specimen (70°F to 90°F).

The junction temperature difference for the high temperature runs with the better insulating materials was usually near 200°F. Thus the uncertainty in h would be:

annealed aluminum	3 Btu/hr ft^2 °F
as received aluminum	2 Btu/hr ft^2 °F
stainless steel	0.3 Btu/hr ft^2 °F

For the low temperature runs these values would be reduced somewhat since the junction temperature difference increased to as much as 400°F for the liquid nitrogen collant runs. Therefore, the energy balance method is preferred for the aluminum specimens when the temperature gradient is less than 1-1/2 °F/inch, which corresponds to an approximate value of h of 7 to 9 for the high temperature runs. Although a heat balance was performed for the stainless steel specimens the heat

calculated from the thermal conductivity is preferred. Besides improving the ability to calculate the heat transfer, the stainless steel specimens provided a means to test the effect of surface hardness on the junction thermal resistance with interstitial materials. Except for wire screens this effect appeared to be negligible.

The primary purpose of a low conductance interstitial material is to minimize the heat transfer for a given temperature difference, or $Q/\Delta T$ should be a minimum. If surface contact effects are neglected and a linear temperature gradient is assumed,

$$Q = hA\Delta T = k_e A \frac{\Delta T}{\ell}$$

Thus,

$$k_e = h\ell$$

A good thermal insulating material would therefore have a very low value for the product $h\ell$. This is compared for all of the materials tested as a function of pressure in Fig. 6. The compression strain values used to calculate ℓ were obtained at room temperature, and some deviation in these values could be expected at higher or lower temperatures depending on the expansion or contraction of the interstitial material with temperature. Since the sides of the disk are free, it was assumed that any possible deviation can be neglected for the comparison of materials in Fig. 6.

In some applications the insulation weight may be important. This implies that the effective density of the material, ρ_e, be a minimum. Combined equally with the ther-

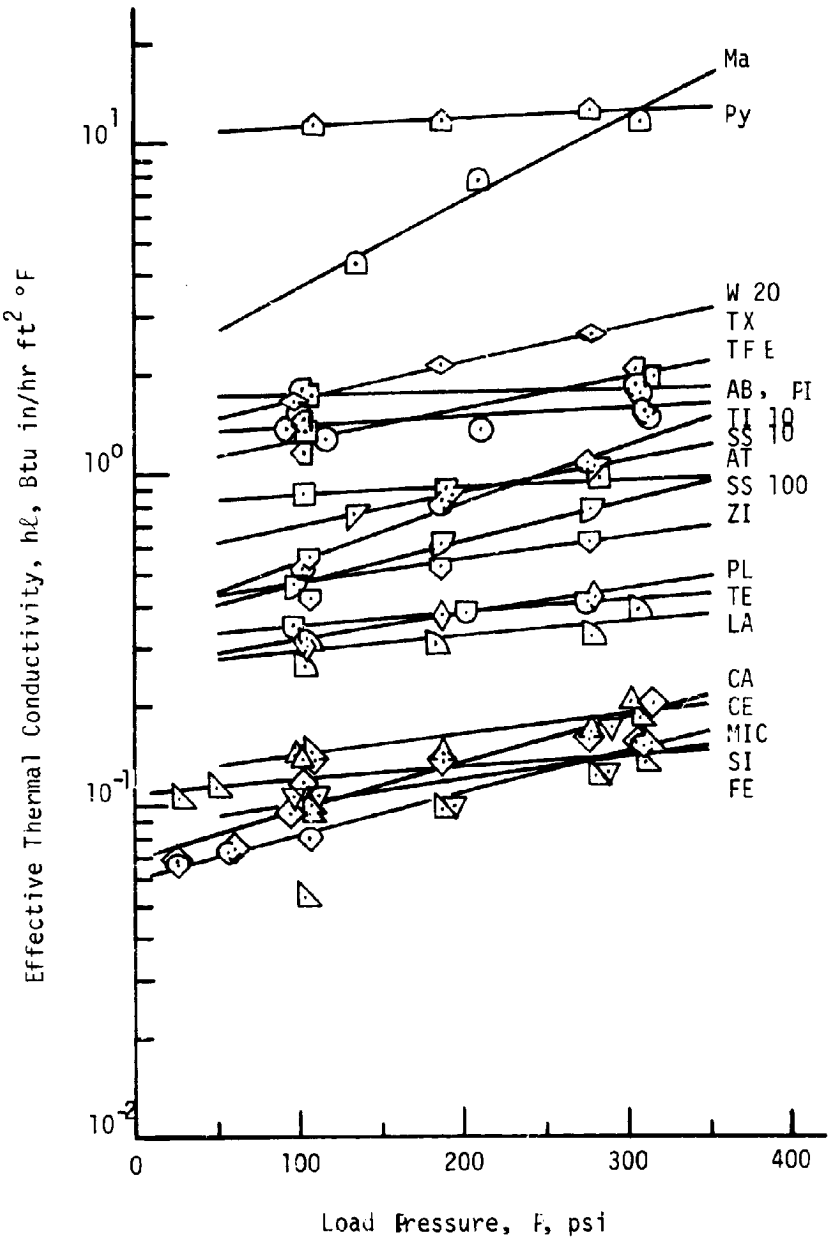

FIGURE 6. Effective Thermal Conductivity Curves

mal criterion this suggests that the product

$$k_e \rho_e = \frac{kW}{A}$$

be a minimum. Since all test samples had the same cross-sectional area, the product hW is plotted in Fig. 7. An in vacuum weight was obtained with a Cahn Electrobalance for the fibre paper and laminated board materials. Since 1/h is proportional to the thermal resistance the product hW in Fig. 7 can be interpreted as the mass per unit thermal resistance. Thus, this value would be a minimum for the better insulating materials.

In any installation where a compressive load is applied the mechanical strength of the material must be considered. In static cases the compression strain curves (Fig. 5) indicate the degree of compression. However, for cyclic load and temperature conditions the material should be subjected to a variable load test. Carbon paper, ceramic paper and felt were run in a cyclic load test to failure since their mechanical strengths were the most questionable of the better materials indicated by Figs. 6 and 7. Silica paper was not considered due to the discoloring at higher temperatures. The ceramic paper when cycled between 10 and 500 pounds six times and the felt when cycled four times between 10 and 800 pounds were found to disintegrate. On the other hand, carbon paper which was also cycled six times between 10 and 500 pounds did not fail but was compressed to approximately one-half of its initial thickness.

The effect of initial compression of the sheet materials was illustrated with the WRP-X-AQ felt. First a series of thermal tests were run with increasing load pressure to

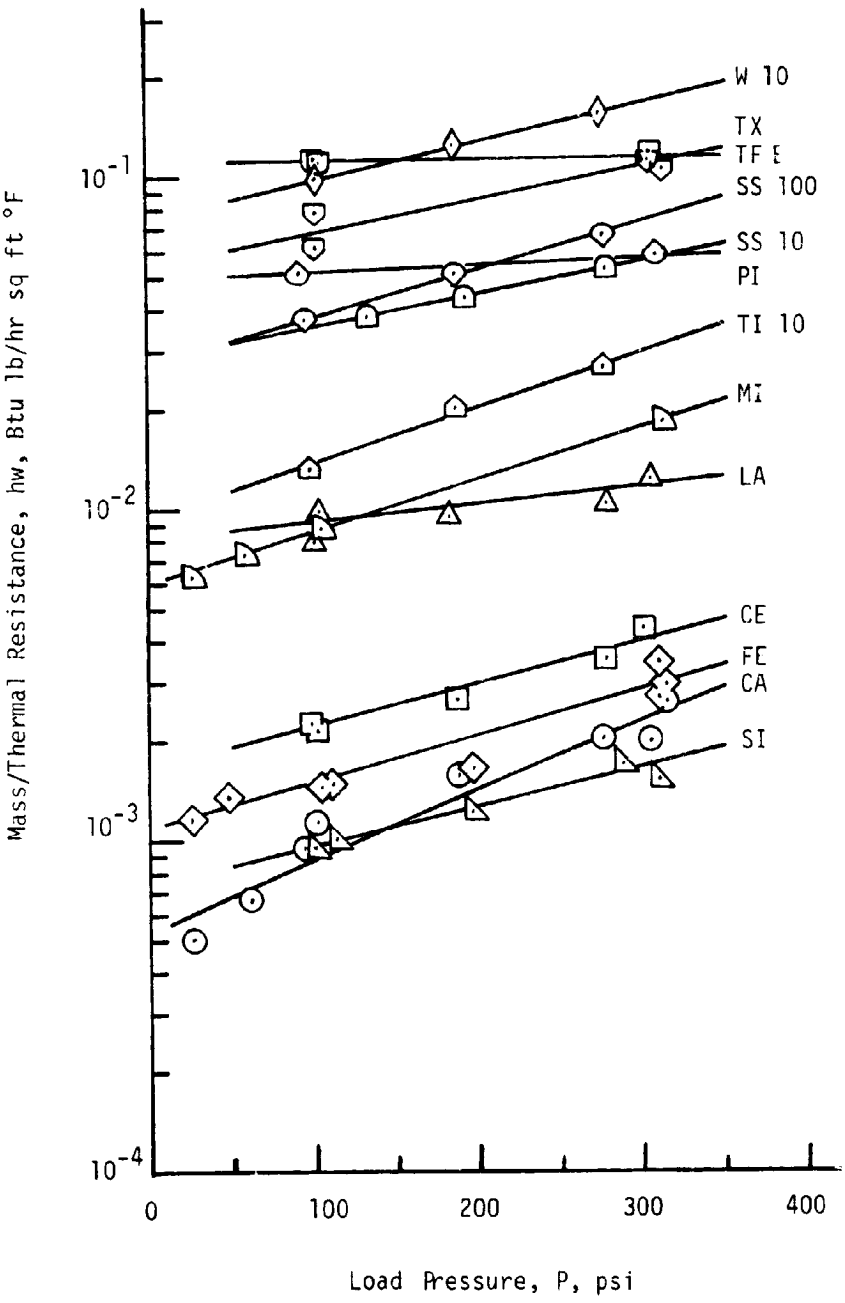

FIGURE 7. Mass Per Thermal Resistance Curves

1000 psi, then return runs at 550 psi and 100 psi were taken. The increases in conductance over the initial increasing load runs were 50.3 percent and 233 percent, respectively. Also the effect of the metal specimen surface roughness was briefly considered. The low temperature specimen surface was artificially roughened with a lathe cut to 200 μ-inches. Subsequent runs with asbestos board and carbon paper did not deviate from the previous smooth surface results. This was expected since these particular materials demonstrate a thermal resistance due to a bulk material resistance, i.e. ℓ/kA, and not a surface contact effect. Further, for mica a small effect was observed which would again emphasize the surface effect demonstrated by mica.

As a result of the different behavior of carbon paper and mica in the compression tests, multilayer thermal tests of these materials were conducted. Five layers of mica (overall 0.0178 inches) and six layers of carbon paper (overall 0.330 inches) were run at load pressures of 100 psi and 300 psi. Within the experimental uncertainty the product, $h\ell$, for carbon paper for the single layer and the six-layer tests was constant, i.e. k_e a constant value at a given pressure. In contrast to this the same comparison for mica indicates that the product, $h\ell$, increases with the number of layers which again suggests that a surface contact resistance effect is predominant for mica.

Since the heat transferred between metal surfaces is significantly influenced by small variations in the contact area. the insulating effect of a geometric resistance is obvious Perforated sheets, roughened or corrugated surfaces, or wire screens represent such materials. Three different

wire screen materials were tested; tungsten, W, titanium, Ti, and stainless steel, SS. Results for these tests are included in Figs. 6 and 7 with the mesh size denoted as 10, 20, or 100/inch. It can be assumed that contacts with the bounding metal surfaces of the junction gap occur at the points where the wire weave of the screen overlap. For a 100 mesh screen there would be approximately 10^4 contacts per square inch but for a 10 mesh size only 10^2 contacts per square inch. Thus the larger thermal resistance of a 10 mesh screen over that for a 100 mesh screen would be expected. However, the wire diameter is reduced with increased mesh size, hence a smaller area per contact. For this reason Table 3 was presented to compare the thermal resistance per contact for the runs with the aluminum specimens. Several runs with stainless steel screens and stainless steel specimens were added in Part IV.

As a result of the earlier comparison tests, the seven materials which had the lowest h values (Fig. 3) were rerun with specimen sets 3 and 4 (Table 2) to check the repeatability of the experimental results. The repeat runs were conducted for both the high and low junction temperatures and the calculated h values agreed closely with the comparative runs except for mica. The second series of runs for mica were approximately 50 percent lower than the comparative test series. The test samples were obtained from a local heater manufacturer and were considered an economy grade. Areas of discoloration were visible in the mica sample. These were either black-gray or reddish-brown in color and indicate the presence of impurities such as silicon or iron oxides. Another test sample from the same batch of mica sheets with a black-gray instead of the reddish-brown discoloration was

TABLE 3

TABULATED EXPERIMENTAL DATA
FOR WIRE SCREEN

RUN NO.	WIRE DIA. in.	T_m °F	LOAD/CONTACT lb.	RESISTANCE/CONTACT Hr °F/Btu
2-SS10-16	0.025	192	1.32×10^{0}	8.32×10^{2}
2-SS10-17	0.025	190	1.92×10^{0}	7.39×10^{2}
2-SS10-18	0.025	191	2.79×10^{0}	6.02×10^{2}
3-SS10-23	0.025	-106	1.04×10^{0}	1.95×10^{3}
3-SS10-24	0.025	-104	2.99×10^{0}	1.13×10^{3}
1-SS100-57	0.004	216	0.96×10^{-2}	2.23×10^{4}
1-SS100-58	0.004	220	1.87×10^{-2}	1.60×10^{4}
1-SS100-59	0.004	229	2.77×10^{-2}	1.56×10^{4}
1-TI10-60	0.025	195	1.02×10^{0}	13.45×10^{2}
1-TI10-61	0.025	192	1.86×10^{0}	8.83×10^{2}
1-TI10-62	0.025	189	2.75×10^{0}	6.58×10^{2}
1-W20-64	0.007	218	0.25×10^{-1}	4.88×10^{2}
1-W20-65	0.007	229	0.47×10^{-1}	3.79×10^{2}
1-W20-66	0.007	246	0.69×10^{-1}	3.10×10^{2}
6-SS100-43	0.004	249	1.04×10^{-2}	4.49×10^{4}
6-SS10-45	0.025	234	1.03×10^{0}	19.46×10^{2}
7-SS100-49	0.004	-35	1.00×10^{-2}	6.58×10^{4}
7-SS100-50	0.004	-17	3.04×10^{-2}	3.12×10^{4}
7-SS10-51	0.025	-66	1.06×10^{0}	23.15×10^{2}
7-SS10-52	0.025	-53	3.05×10^{0}	14.02×10^{2}
7-SS100-53	0.004	293	1.05×10^{-2}	4.39×10^{4}
7-SS100-54	0.004	236	1.00×10^{-2}	4.39×10^{4}
7-SS100-55	0.004	254	3.04×10^{-2}	2.25×10^{4}
7-SS10-56	0.025	217	1.03×10^{0}	20.51×10^{2}
7-SS10-57	0.025	219	3.07×10^{0}	11.25×10^{2}

tested. In this third run at 100 psi the h value was increased to 83 percent of the first run. After cleaning the aluminum specimen surfaces another mica sample of the same type was re-run at 100 psi and the resulting h value for this fourth run was 96 percent of the initial value. Although the low h values for the second run series could be somewhat attributed to contamination of the aluminum surfaces, it seemed more likely that the differences in the mica samples and perhaps possible misalignment of the test column were more probable reasons. To avoid a problem of variations in the test samples a clear grade of mica (optically clear) was used in all remaining tests with mica including those in Parts IV and V.

In summary, based on the criteria of low conductance and minimum weight the carbon paper proved to be the better material. However, if mechanical strength is of primary importance, wire screens should be considered. The highly compressible materials such as carbon paper demonstrate a thermal resistance which is a function of the bulk material resistance (ℓ/kA); whereas, harder surface materials such as mica evidence a strong dependence on a surface contact effect.

CHAPTER III

INTERSTITIAL MATERIAL AND MULTILAYER TESTS

The test results for the additional interstitial material and bare junction runs which were conducted during Part IV are listed in Appendix A. The test runs were designated by several symbols to specify the metal test specimen set, the interstitial material, and the run number in chronological order for a particular specimen set. For examples, run 7-MICP-7 refers to the seventh run with specimen set 7 and a single layer of perforated clear grade mica, and 6-SS100L-44 is the 44th run with set 6 and two layers of 100 mesh stainless steel screen. The screens were oriented at 45 degrees to one another for the two layer tests.

Comparative tests for textolite, pyrotex and TFE teflon sheets were run in preparation for their possible use as bolt insulating materials in Part V. The supplier, manufacturer's data and initial thicknesses of materials for the thermal tests are listed in Table 1. The effective thermal conductivities, $h\ell$, are plotted for comparison with the other materials in Fig. 6. Although the magnitudes of $h\ell$ are relatively large for all three materials the teflon and pyrotex demonstrate the desirable feature of a small dependence of h on the load pressure, for the range 100 to 300 psi. Repeat runs with textolite and teflon agreed very closely except for run 7-TX-44. Test samples for textolite, which is a hard glass laminated sheet, had to be cut on a mill. Without extreme care and a sharp cutting tool the edges break apart slightly. Some evidence of this existed with the sample for run 7-TX-44. Another sample was carefully machined to avoid this problem and the results of 7-TX-45 and -46 agree

more closely with the initial runs 6-TX-31 and -32. Disagreement at the lower pressures could be attributed to the surface effect which is reduced with increased load pressure. Thus it can be concluded that the thermal resistance of textolite is a combination of surface contact and bulk material effects. In earlier tests with teflon (2), indicated by the symbol TE in Fig. 6, a 0.0028 inch thick sheet of FEP teflon was used. In Part IV the interest was to test materials of greater thickness for application in Part V. Unfortunately the vacuum balance was not available so the weights in air were used to calculate hW for Fig. 7. On a weight basis these materials are comparable to the wire screens.

In an earlier study (10) it was found that dusting contacting stainless steel surfaces with manganese dioxide powder resulted in a large increase in the thermal resistance over that for the bare surfaces. Thus, as another comparison, a very thin layer of rutile powder was placed on the stainless steel specimen surfaces. To provide a more definitive measure of the powder, it was separated between 0.0024 inch and 0.0017 inch sieves. Approximately a single grain thickness layer was spread on the specimen surface, this powder was then collected and weighed (0.15 grams). The same weight of powder was then placed on the specimen surface for testing. The powder is crushed into a layer with increased loads with a resulting large increase in h. Bare junction runs were intermixed with the material runs to test for variations in the metal test specimen surfaces. Run 6-BJ-38 followed the rutile powder tests. The surfaces were wiped clean but the approximate 30 percent reduction in h can be directly attributed to the con-

tamination of the surface by the two previous runs with rutile powder. Thus dusting of the surfaces can easily produce sizeable variations in the junction thermal resistance.

The multilayer test results for mica in Part III had shown that the thermal conductance was greatly dependent upon a surface contact effect. To demonstrate the dependence, tests with one, two, and three layers of mica were conducted. The results for these tests along with the data for five layer tests which were reported in Reference 3 are graphed in Fig. 8. A linear dependence of h on the load pressure seems evident. The repeated runs generally agree within the experimental uncertainty except for the two layer case at 100 psi. At any particular pressure each test point was obtained for a new test sample. Since the thermal resistance for mica is a function of the surface contact, the most probable reason for this disagreement is the possibility of changes in the surface conditions of the mica layers and the metal specimens. Run 7-MIC2-37 is a return pressure test point for the same test sample as run 7-MIC2-35. Also run 7-MIC3-41 is a repeat of 7-MIC3-39. For both cases nearly the same values of h were obtained (Appendix A). Thus a precompression of the test sample does not seem to materially affect the thermal conductance.

The junction thermal resistance can be defined as,

$$R = 1/hA$$

The values for 1/h-RA and ℓ for the multilayer tests were calculated and plotted in Fig. 8 for 100 and 300 psi loads. A value for ℓ was found from the compression strain curves (Fig. 5) and the measured initial thicknesses of the test samples. As a simplified analogy for these curves the total

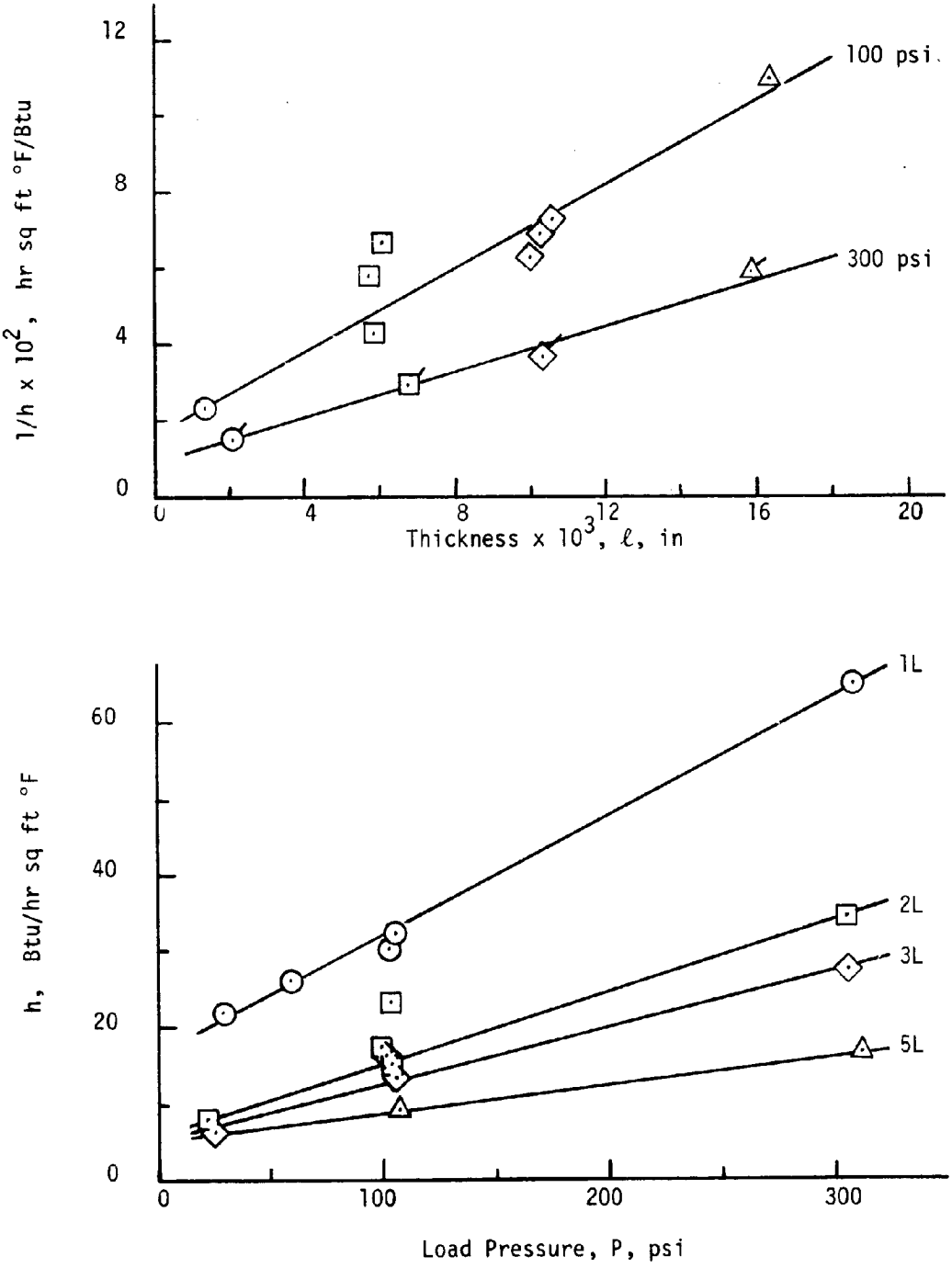

FIGURE 8. Multilayer Mica Test Results

junction resistance can be supposed to be a sum of the contact resistance between the mica and the metal specimen, R_C, the contact resistance between the mica layers, R_M, and a bulk material resistance of ℓ/kA.

$$R = 2R_C + (n-1)\ R_M + \frac{\ell}{kA}$$

where n represents the number of layers. If each layer is of the same thickness ℓ_1 then, $\ell = n\ell_1$. At a constant pressure and temperature ℓ_1 and k would remain constant, therefore,

$$1/h = A(2R_C - R_M) + \left(\frac{A}{\ell_1} R_M + \frac{1}{k}\right)\ell$$

Futher, for these conditions R_C and R_M would be constant. A linear function of this type is indicated by Fig. 8. The decrease in the slope with pressure can be explained as a reduction in R_M and an increase in k for layer compressive loads.

Variable thickness samples of laminate T-30LR were tested to compare the results to a multilayer sample of the same initial thickness and weight. The calculated value of 1/h is plotted versus the calculated compressed thickness in Fig. 9. A linear function is shown for the same reason as just described for the multilayer mica tests. In this case, however, an intermediate contact resistance was not present except for the three 1/16 inch layer run. Thus, the slope provides a measure of 1/k for laminate compressed to 100 psi. The three layer sample increased the thermal resistance by 50 percent over that for a continuous piece of the same thickness. The value for the nominal 1/4 inch sample was approximately 0.14 hr ft^2 ^oF/Btu greater than the linear curve

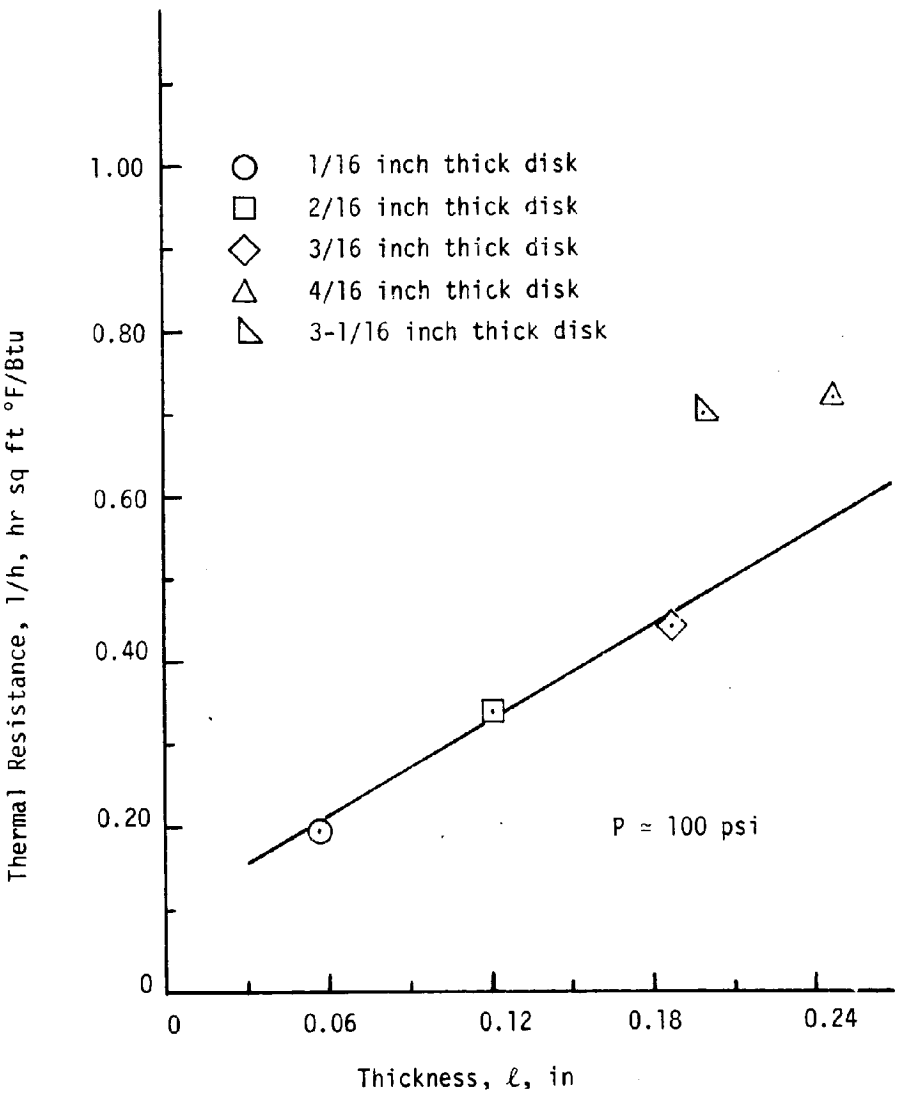

FIGURE 9. Laminate Variable Thickness Results

would predict. Laminate is a hard laminated board and the test samples were machined from a sheet approximately 5/16 inch thick. The major laminations, which form the sheet, are about 1/16 inch thick. After the test run with the 1/4 inch sample one of these laminations was found to have separated. Thus, an internal contacting surface was present during the test. From the three layer result the increase in thermal resistance due to two intermediate contacts is 0.22 hr ft^2 ^oF/ Btu, one-half of which is very nearly equal to the increase noted for the 1/4 inch sample.

Since wire screens are capable of withstanding large compressive loads, additional runs with stainless steel screens against the stainless steel surfaces were conducted. The effective values of the junction thermal resistance, 1/h are illustrated in Fig. 10 to compare the different wire screens and test specimen materials. All of the data are for the higher junction temperature runs. Data for the aluminum surfaces denoted as a -AL in the figure were reported in Reference 3. The thermal resistance for carbon paper (CP) is also included for comparison. As shown the thermal insulation of contacting stainless steel surfaces can be accomplished as well with 10 mesh paper. However the load bearing capacity of the screen is superior to the carbon paper. Slight indentations were noticed in the stainless steel specimen surfaces after the test runs with 10 mesh wire screens. The same type of indentations were quite noticeable in the aluminum surfaces. Therefore part of the increase in thermal resistance for stainless steel surfaces can be attributed to a reduction in the contact area, but the primary effect seems to be the large decrease in thermal conductivity, a factor of 10 from aluminum to stainless

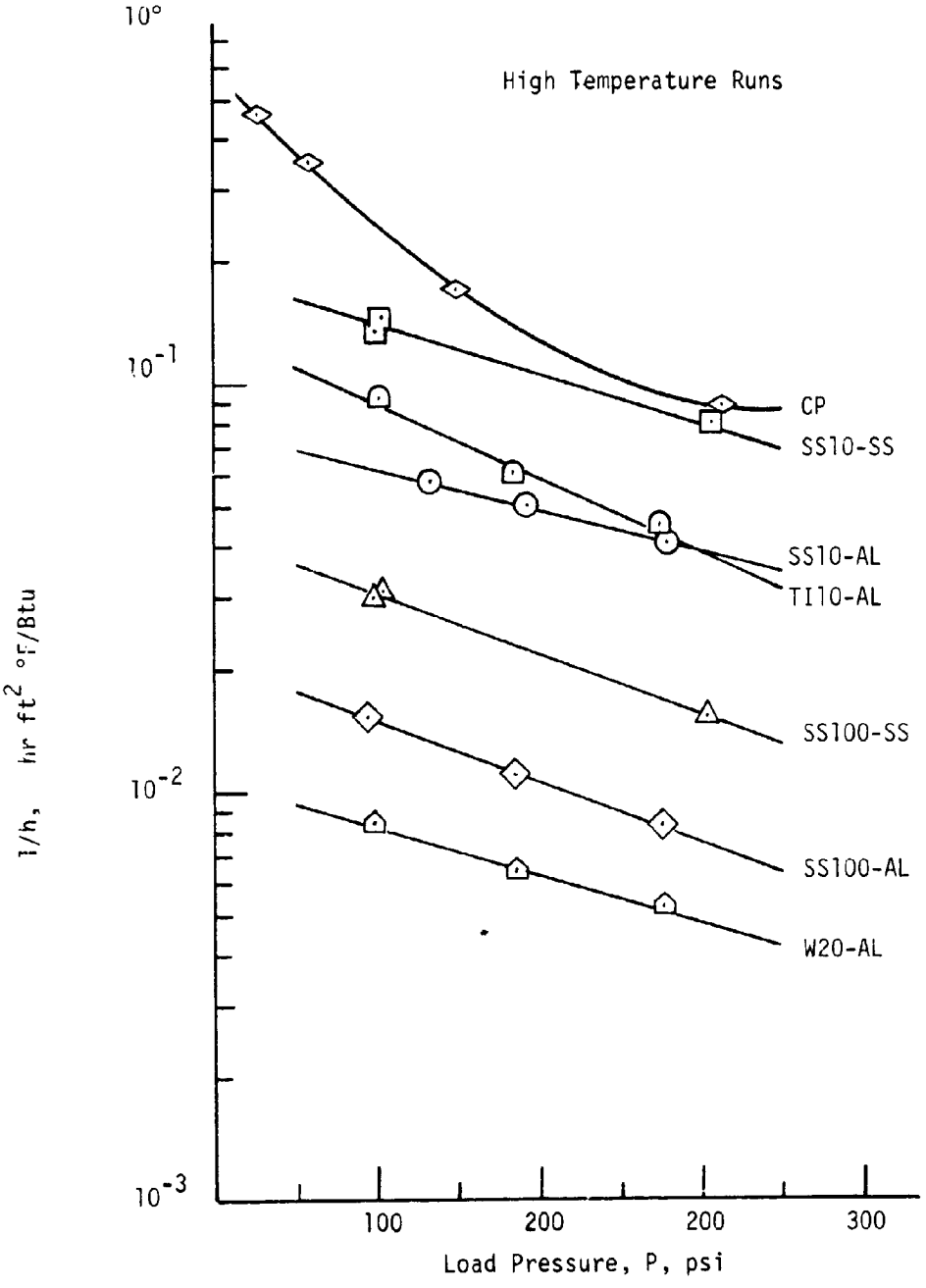

FIGURE 10. Thermal Resistance of Wire Screens

steel. These same factors can be applied to the 20 mesh tungsten screen. For the range of load pressures from 100 to 300 psi the data indicate an exponential decrease in the thermal resistance for wire screens. In Table 3 the load per contact is

$$L_c = \frac{P}{M^2}$$

where M is mesh size, and the thermal resistance per contact is

$$R_c = \frac{M^2}{h}$$

It is assumed that the contacts occur at the points where the wire weave overlays and that the resulting contacts are in parallel. The increased thermal resistance for lower thermal conductivity wire, smaller wire diameter, lower temperatures, and stainless steel surfaces are apparent.

The effects of reducing the contact area by perforating layers of mica and 0.001 inch stainless steel shim are shown by runs 6-MICP-39 and -40, 7-MICP-7, and 6-SH-41 and -42. Approximately 25 percent of the area was removed with a No. 45 drill. The disk was divided into three equal area segments and the same number of holes were drilled in each region. The lower value of h for run 6-MICP-39 as compared with run 7-MICP-7 may be a result of the same difficulty encountered for the bare junction run 6-BJ-38. The possible surface contamination with rutile powder could have an effect on the contact resistance for mica. Another very possible explanation could be the presence of rough edges left by the drilling operation. Nevertheless a reduction of at least 40 percent in the magnitude of h at 100 psi can be obtained by the area reduction. On the other hand, the reduction in area for the stainless steel shim seems to have had almost a negligible effect.

Several multilayer tests with two layers of mica and a variable intermediate material were performed at a load pressure of 100 psi (Table A-2). For reference an excerpt of the experimental results is given in Table 4.

TABLE 4

COMPARISON OF MULTILAYER COMBINATIONS

Run	Intermediate Material	h Btu/hr ft^2 $^\circ$F
7-MIC3-10	Mica	15.8
7-MIC3-10	Mica	14.4
7-MIC3-39	Mica	13.6
7-MIC3-41	Mica	13.5
7-$^{MIC2}_{SH}$-28	0.001 S.S. shim	14.8
7-$^{MIC2}_{SHP}$-29	0.001 S.S. shim (75% area)	9.3
7-$^{MIC2}_{MICP}$-30	Mica (75% area)	12.6
7-$^{MIC2}_{MICP}$-31*	Mica (75% area)	12.8
7-$^{MIC2}_{SS100}$-32	100 mesh S.S. screen	9.0
7-$^{MIC2}_{SS100}$-33*	100 mesh S.S. screen	11.1

all runs at 100 psi load pressure
average mean temperature, 245°F
* initially compressed to 800 psi

The effect of a stainless steel shim is approximately the same as a layer of mica. Also, perforation of the shim has a noticeable effect but a 25 percent area reduction with an intermediate layer of mica has a lesser influence. Therefore, it could be surmised that the surface contact resistance between mica surfaces is somewhat smaller than between mica and a stainless steel surface. Insertion of a 100 mesh stainless steel screen reduces the thermal conductance to one-half of that obtained with two layers of screen oriented at 45 degrees to one another (Run 6-SS100L-44). The pre-compression to 800 psi has a small effect except for the stainless steel screen which penetrates the mica layers.

CHAPTER IV

INSULATION OF FLANGE JOINTS

Two antenna assembly bolted flange joint configurations were selected to test with interstitial insulating materials. In a typical application the upper flange (Figures 11 and 12) would be attached to a relatively large surface. Therefore the base flange was constructed somewhat larger than the upper flange to provide a closer simulation of the actual installation. The flanges were machined from aluminum 6061 stock. In the vacuum chamber the flange sections were fastened to one-inch diameter metal support rods which were instrumented with three centerline (1/2 inch apart) and two surface thermocouples for the purpose of calculating the heat transfer. The installation of the thermocouples was accomplished in the same manner as the metal test specimens used for the interstitial material tests. For both flanges the ends of the one-inch diameter shank were cut down to a smaller diameter and inserted into a cylindrical cavity drilled into the end of the respective support rod. They were fastened into position by set screws. The mating surfaces were coated with a mixture of aluminum powder and vacuum grease to reduce the thermal resistance between the support rod and the flange. One support rod was threaded into the heat sink (Fig.13) and the other was machined with an enlarged diameter (1-1/2 inch) at one end to which the band heater was fastened. The other details of the support rods and radiation shields were the same as for the metal test specimens used in the earlier tests.

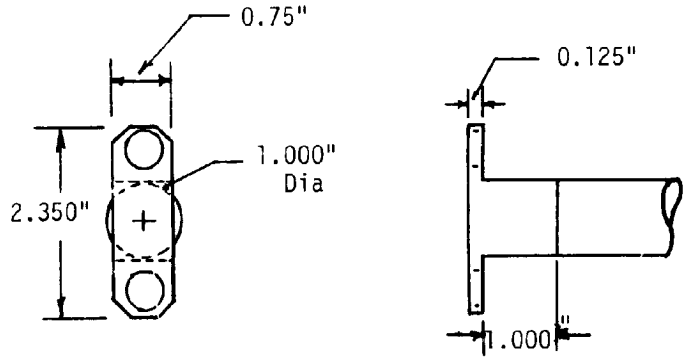

UPPER FLANGE

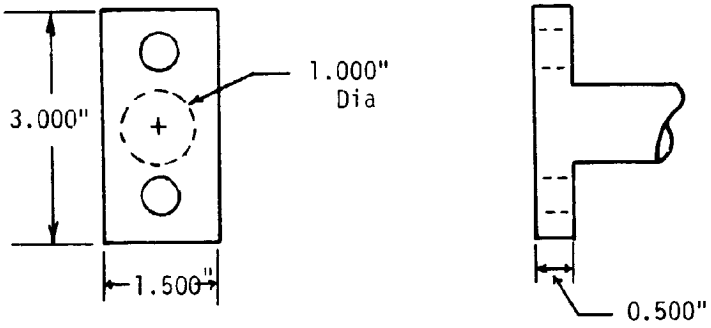

BASE FLANGE

FIGURE 11. Two Bolt Flange Joint

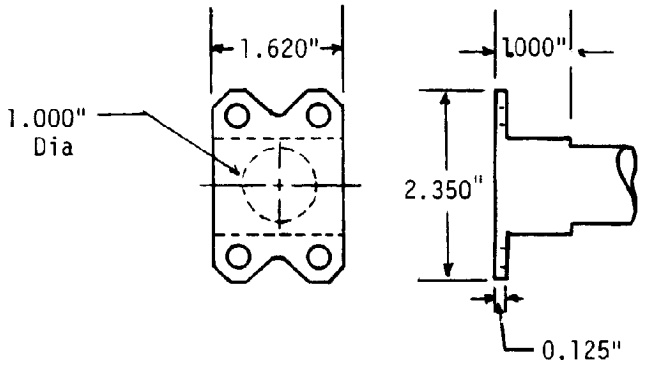

UPPER FLANGE

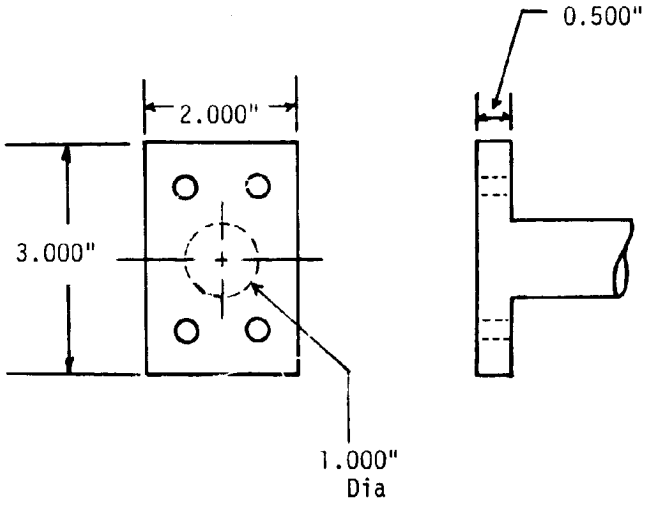

BASE FLANGE

FIGURE 12. Four Bolt Flange

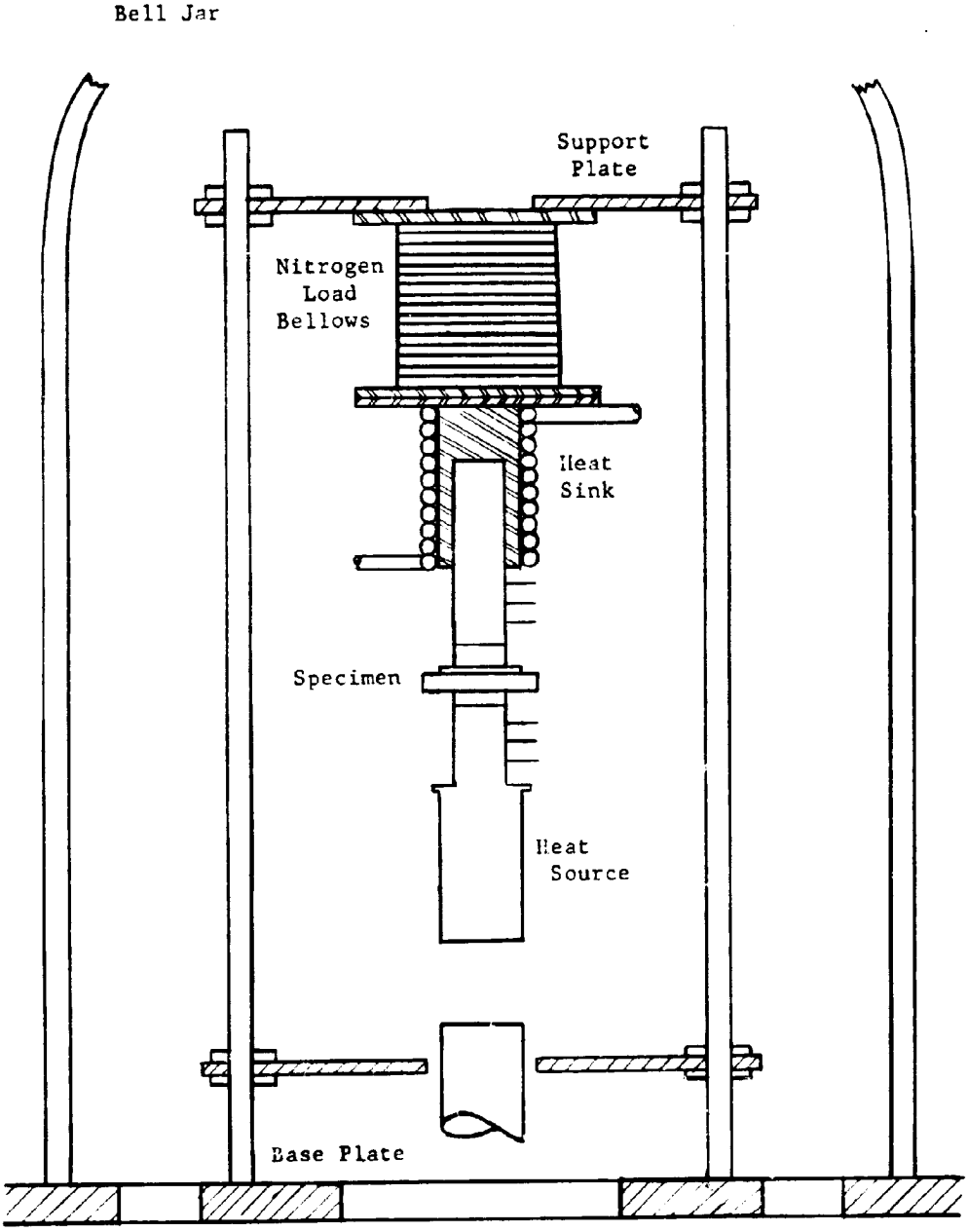

Figure 13. Schematic Diagram of the Flange Joint Installation

To measure the heat transfer rate over a wide range of magnitudes the instrumented support rods were constructed from armco iron and stainless steel 304. For the uninsulated flange (higher heat flux) the armco iron set of heat metering rods were installed and for low heat flux runs the stainless steel set was substituted. Two holes, one on either side of the flange shank, were drilled (No. 56 drill) from the back face of the flange to within 0.005 inch of the mating surfaces. Copper-constantan thermocouples were inserted to obtain some measure of the temperature difference across the flange junction. The two thermocouples on each flange agreed within $2^{o}F$ of one another for all of the test runs. The average of these readings was taken as the flange temperature and subsequent values of the temperature difference ΔT and the mean temperature T_m were calculated (Tables A-3 and A-4 in Appendix A). The heat transfer rates were calculated by the product of the thermal conductivity and temperature gradients for the heat metering support rods. In the table of results Q_H refers to the heated side and Q_C to the cooled side of the flange installation. Run numbers specify the flange test set, whether two bolt or four bolt, and the chronological run number. For an example, 2-2BT-4 is the second two bolt flange set (upper flange and base flange) and the fourth run with this set. Various combinations of bolt and flange face insulations were tested for comparison with the two bolt flange configuration. Following these runs, carbon paper and 100 mesh stainless steel screen insulations were tested with the four bolt flange. The symbols in Tables A-3 and A-4 used to describe the type of insulation are defined in Table 1. The uninsulated case is denoted as BJ. With the exception of the textolite, pyrotex,

and teflon bolt insulating washers listed in Table A-3 all insulating materials were the same thickness as the samples for the earlier interstitial material tests. Face insulating layers were cut to fit the upper flange surfaces, except the center portion of the intermediate layer of stainless steel shim in runs 1-2BT-23 and -24 was removed.

The first seven runs listed in Table A-3 (1-2Bt-1 through 1-2BT-7) were preliminary performance runs. Bolt torque was 15 in-lb and for runs 2 and 4 of the series, an additional axial load of 100 psi was applied. The cooling fluid was water for all runs with the two bolt flange with the exception of runs 1, 2, 6 and 7 for this series, during which liquid nitrogen was the coolant.

In order to compare the performance of different insulation combinations an effective thermal conductance $Q/\Delta T$ was defined for the flange tests. This parameter is plotted versus T_m in Figures 14 and 15. The two uninsulated run series, 1-2BT-8 through -11 and 2-BT-1 through -4, are compared in Figure 14. Even though the bolt torque was greater for set 2, 25 in-lbs as compared with 15 in-lbs, the thermal conductance is much less than for set 1. Some surface variation could be encountered from the machining operation, a mill cut, but in addition set 1 was run through the preliminary tests so the surface contact may have been improved. After run 11 the bolt attachment holes in the upper flange of set 1 were chamfered at 45 degrees and insulating washers of textolite, pyrotex, and teflon were machined to fit the chamfer. The threaded portion of the bolt, near the bolt head, was cut down to avoid contact with the upper flange and the bolts were threaded into the base flange. Test results for the comparison

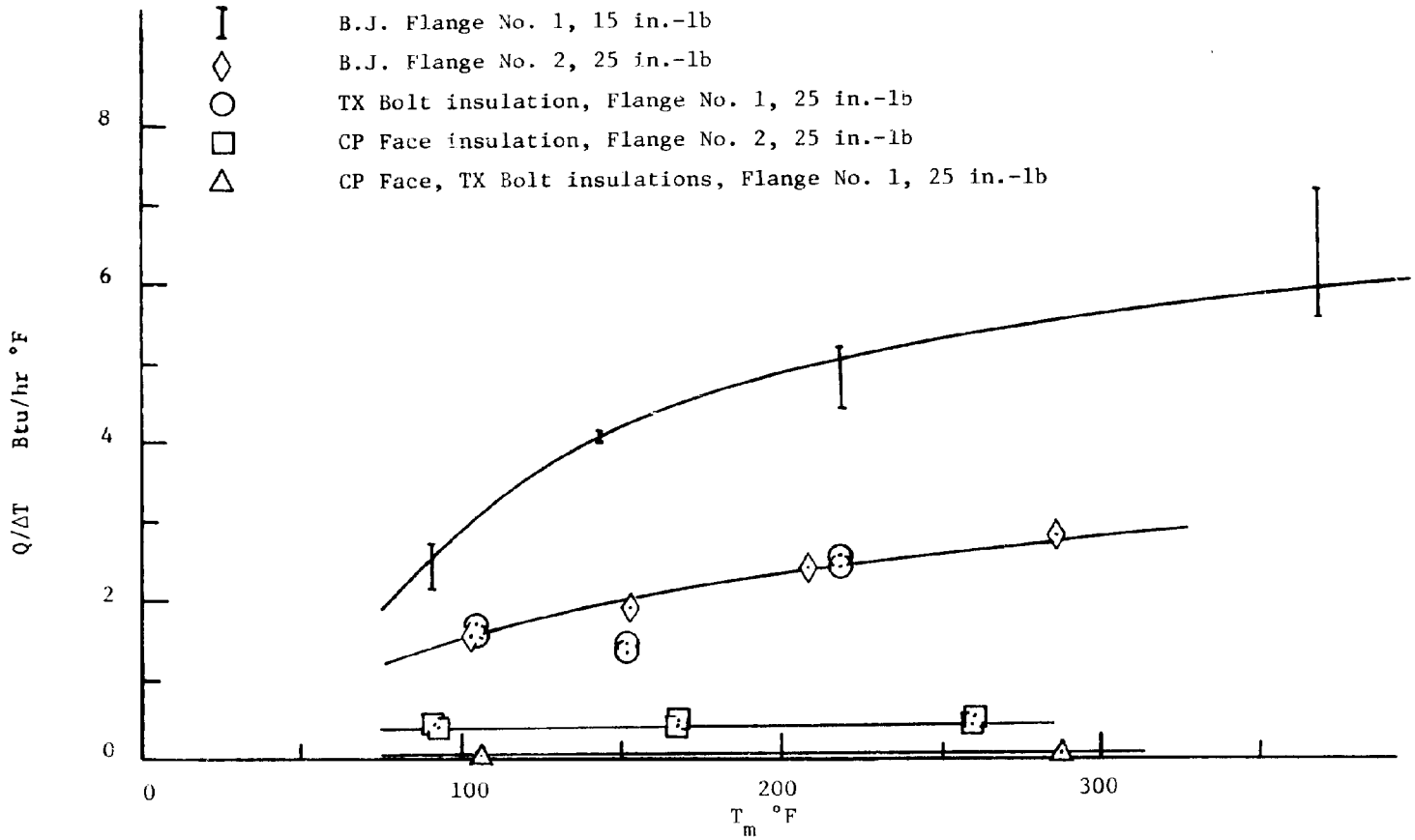

FIGURE 14. Thermal Conductance Comparison for Two Bolt Flange

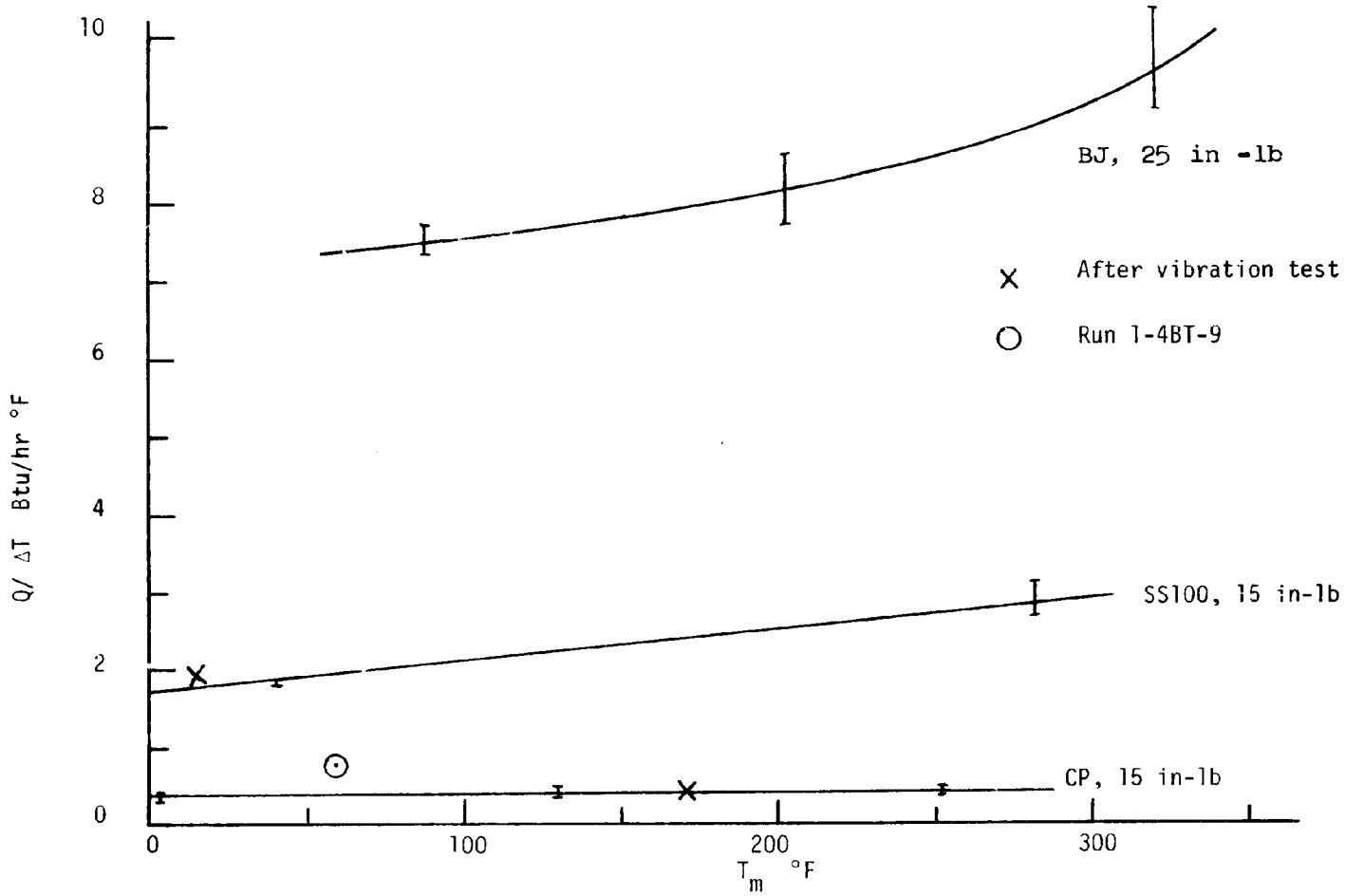

FIGURE 15. Thermal Conductance for the Four Bolt Flange

runs 1-2BT-12 through 1-2BT-16 in Table A-3 are also included in Fig. 14. Although insulation of the bolts has a very noticeable effect the insulation of the flange face with a single layer of carbon paper reduces the effective thermal conductance by a factor of from 2-1/2 to 5 over the uninsulated case. The values of $Q_H/\Delta T$ and $Q_C/\Delta T$ are indicated by the bands plotted in Figure 14. With both bolt and face insulation the conductance was reduced to 0.05 and 0.08 Btu/hr $^{\circ}$F. The remainder of the runs with the two bolt flange configuration were conducted to test several different insulation combinations. The calculated conductance for these tests are tabulated in Table 5.

TABLE 5

TWO BOLT FLANGE COMPARISON

Run Number	$Q_H/\Delta T$ Btu/hr$^{\circ}$F	$Q_C/\Delta T$ Btu/hr$^{\circ}$F	Insulation Face	Insulation Bolt	Bolt torque, in-lbs Initial	Final
1-2BT-17	0.17	0.12	CP	TX	50	20
1-2BT-18	0.12	0.08	CP	PI	25	10
1-2BT-19	0.23	0.17	CP	PI	50	32
1-2BT-20	0.16	0.12	CP	TFE	25	5
1-2BT-21	0.26	0.20	CP	TFE	25	12
1-2BT-22	0.28	0.21	CP	TFE	50	25
1-2BT-23	0.73	0.55	MIC2 SH	TFE	25	5
1-2BT-24	0.31	0.24	MIC2 SH	TFE	50	--

TABLE 5 Cont'd.

Number	$Q_H \Delta T$ Btu/hr°F	$Q_C \Delta T$ Btu/hr°F	Insulation Face	Insulation Bolt	Bolt torque, in-lbs Initial	Final	
1-2BT-25	0.42	0.32	SI	TFE	25	5	*
2-2BT-8	0.33	0.25	CP	MIC SH	25	15	*
2-2BT-9	0.17	0.12	CP	TX	25	10	
2-2BT-10	0.33	0.26	CP	SH SS100	25	15	*
2-2BT-11	0.37	0.28	TX	SH SS100	25	10	
2-2BT-12	0.74	0.58	SS100	SH SS100	25	--	
2-2BT-13	0.84	0.67	SS100	SH SS100	25	10	
2-2BT-14	0.98	0.77	SS100	SH SS100	25	--	

*Axial load of 500 psi applied before setting torque

From Table 5 the decrease in thermal conductance for all of the insulation combinations over that for the uninsulated case is evident. However the carbon would be the better choice for a flange face insulating material and the chamfered insulating washers for the bolt. The bolt breaking torque was checked after each run. These values are listed in Table 5 as the final bolt torque. For runs with insulating materials the bolt torque was reduced considerably as a consequence of the thermal stresses encountered during the test runs. This particular problem can be alleviated by several means. For example, the material can be pre-stressed and

TABLE A-2 (Cont'd.)

Run	P	T_m	ΔT	h
	Psi	^oF	^oF	Btu/hr sq ft ^oF
Special Multi-Layer Test (Cont'd.)				
$7-{}^{MIC2}_{MICP}-30$	104	241	193.5	12.6
$7-{}^{MIC2*}_{MICP}-31$	104	240	193.9	12.8
$7-{}^{MIC2}_{SS100}-32$	103	241	221.6	8.95
$7-{}^{MIC2*}_{SS100}-33$	102	234	198.9	11.1

* Material initially compressed to 800 psi

tension washers can be added. These solutions were tested with the four bolt flange with the result of no measurable decrease in torque. Also the bolt material could be the same as the flange and threaded insulating inserts could be installed in the base.

Vibration tests were run with two insulating combinations for the two bolt flange. In both cases the face insulation was a single layer of carbon paper and a chamfered washer, one textolite and the other teflon. The flanges were attached to a shaker table in a vertical position and the oscillation frequency was varied slowly from zero to 2000 cps over a period of two minutes. An initial bolt torque of 25 in-lbs was applied in both cases. In each case the breaking torque was reduced to 15 and 20 in-lbs for the two bolts. Similar tests were performed for the four bolt flange, then without disturbing the torque, a thermal test was rerun. These test points are indicated in Figure 15. After the thermal test the final bolt torque was checked and in all cases for the four bolt flange there was no reduction in the bolt torque.

The effective junction thermal conductance for the four bolt flange configuration is illustrated in Fig. 15. The uninsulated tests were run with a bolt torque of 25 in-lbs, all other with 15 in-lbs. Before run 1-4BT-4 and run 1-4BT-9 the flange and insulation were compressed by a 1000-pound load applied in a tensile testing machine. For run 1-4BT-8 the torque was initially set to 100 in-lbs and then reset to 15 in-lbs for the thermal test. From Fig. 15 the carbon paper insulation demonstrates a very desireable trait of small thermal conductance which is essentially unaffected by the mean temperature.

CHAPTER V

SUMMARY

The thermal insulation characteristics of the interstitial materials listed in Table 1 were investigated. Experimental results are reported herein and in previous reports (1, 2 and 3). Selection criteria on the bases of material thickness, $h\ell$ (Fig. 6) and weight, hW (Fig. 7) were proposed. With these comparisons and the additional test of compression under a large cyclic load, the carbon paper was selected as the better material. Geometric resistances, such as wire screen or multilayer configurations, should be considered if mechanical strength is of primary importance. The junction thermal resistance with an interstitial material was found to be a function of the contact surface and the thermal resistance of the material (ℓ/kA). Some materials, notably mica, evidence a strong dependence on the surface contact effect. However, other materials such as carbon paper depend solely on the material resistance. The insulation of aluminum surfaces with wire screen can be measurably improved by separating the screen from the surface with a stainless steel shim. Dusting the mating surfaces with a powder, although difficult to control, will also improve the thermal isolation. Some materials offer the advantage, for prediction purposes, of a small dependence of $h\ell$ on load pressure (Fig. 6). Several examples are pyrotex, asbestos board, and TFE teflon.

The insulation of bolted flange joints can be effectively accomplished by a single layer of carbon paper inserted between the mating surfaces and by textolite bolt

insulating washers (Fig. 14). A difficulty which can be encountered is the reduction in bolt torque, hence the mechanical strength of the joint by compression of the insulating materials as a result of thermal stress or vibration. Precompression of the insulated joint and the use of tension washers proved to be a satisfactory solution. The initial compression of a joint insulated with wire screen has the additional advantage that the contact area would not change appreciably with load.

Further study should be directed to the consideration of new materials and to methods for predicting the experimentally derived values. The present investigation only touched upon possible geometric and multilayer configurations and the use of powders. Thus many variations in test conditions, contact surfaces, joint configurations, etc. should be considered.

BIBLIOGRAPHY

1. Smuda, P. A., L. S. Fletcher, and D. A. Gyorog. "Heat Transfer between Surfaces in Contact: The Effect of Low Conductance Interstitial Materials; Part I: Experimental Verification of NASA Test Apparatus", NASA CR 73122, June, 1967.

2. Fletcher, Leroy S., Paul A. Smuda, and Donald A. Gyorog. "Thermal Contact Resistance of Selected Low Conductance Interstitial Materials", AIAA Paper No. 68-31, January, 1968.

3. Smuda, P. A. and D. A. Gyorog. "Heat Transfer Between Surfaces in Contact: The Effect of Low Conductance Interstitial Materials: Part III: Comparison of the Effective Thermal Insulation for Interstitial Materials Under Compressive Loads", Arizona State University, Mechanical Engineering Department, ME-TR-033-3, August, 1968.

4. Abbott, Rudolph Edward. "Experimental Facilities for Investigating Thermal Contact Conductance in a Vacuum Environment". Unpublished Master's report, Arizona State University (Department of Mechanical Engineering), Tempe, 1967.

5. Eldridge, E. A. and H. W. Deem (eds.). "Report on Physical Properties of Metals and Alloys from Cryogenic to Elevated Temperatures", ASTM Special Technical Publication No. 296, April, 1961.

BIBLIOGRAPHY (Cont'd.)

6. Aluminum Company of America, Alcoa Research Laboratories. Through personal correspondence with C. R. Coppersmith, Manager of the Phoenix Office, June, 1968.

7. Goldsmith, A., T. E. Waterman, and H. G. Hirschkorn. Handbook of Thermophysical Properties of Solid Materials, Vol. 2, New York: Pergamon Press, 1961.

8. Touloukian, Y. S. (ed.). Metallic Elements and their Alloys, Vol. I. Lafayette, Indiana: Thermophysical Properties Research Center, Purdue University, 1966.

9. Fry, E. M. "Measurements of Contact Coefficients of Thermal Conductance", AIAA Paper No. 65-662, September, 1966.

10. Mikesell, R. P. and R. B. Scott. "Heat Conduction through Insulating Supports in Very Low Temperature Equipment", Journal of Research of the National Bureau of Standards, 57: 371-379, December, 1956.

APPENDIX A

EXPERIMENTAL DATA

TABLE A-1

TABULATED EXPERIMENTAL RESULTS

BARE JUNCTION SERIES

Run	P Psi	T_m ^oF	ΔT ^oF	h Btu/hr sq ft ^oF
6-BJ-35	100	257	55.6	93.8
6-BJ-38	91	259	73.6	69.3
6-BJ-47	105	264	74.6	64.4
7-BJ-1	105	327	91.8	54.5
7-BJ-2	308	359	17.4	381
7-BJ-3	104	298	82.0	65.6
7-BJ-4	310	310	15.3	457
7-BJ-5	105	296	80.6	68.7
7-BJ-20	104	324	90.5	57.6
7-BJ-21	209	345	29.9	216
7-BJ-22	305	376	21.7	347
7-BJ-24	105	326	79.3	67.4
7-BJ-42	105	277	77.5	64.9

TABLE A-2

TABULATED EXPERIMENTAL RESULTS

INTERSTITIAL MATERIALS

Run	P Psi	T_m °F	ΔT °F	h Btu/hr sq ft °F
		Carbon Paper		
6-CA-30	319	211	172.1	9.98
		Textolite		
6-TX-31	104	247	165.3	18.8
6-TX-32	314	247	122.1	32.0
7-TX-44	103	244	223.0	8.83
7-TX-45	104	239	131.4	24.0
7-TX-46	306	236	103.8	33.9
		Pyrotex 23 RPD		
6-PI-33	94	248	203.1	12.2
6-PI-34	310	249	196.7	13.8
		Rutile Powder		
6-RP-36	91	237	139.1	22.5
6-RP-37	310	237	96.1	47.8
		Mica		
6-MICP-39	101	240	195.9	12.3
6-MICP-40	307	243	170.2	17.6
7-MIC-6	103	255	119.9	30.1
7-MICP-7	103	236	147.9	17.7
7-MIC2-9	100	253	166.3	17.2

TABLE A-2 (Cont'd.)

Run	P	T_m	ΔT	h
	Psi	°F	°F	Btu/hr sq ft °F
		Mica (Cont'd.)		
7-MIC3-10	103	241	162.0	15.8
7-MIC2-26	104	256	136.0	23.4
7-MIC3-27	106	254	190.7	14.4
7-MIC2-34	20	239	230.6	7.88
7-MIC2-35	105	254	190.3	15.02
7-MIC2-36	306	262	123.0	34.8
7-MIC2-37	105	252	190.1	15.3
7-MIC3-38	23	233	236.5	6.71
7-MIC3-39	106	244	195.6	13.6
7-MIC3-40	306	258	143.1	27.3
7-MIC3-41	102	244	194.8	13.5
	Stainless Steel Shim -- .001 inch			
6-SH-41	103	252	77.5	59.5
6-SHP-42	103	249	76.8	56.9
	Stainless Steel Screen -- 100 Mesh			
6-SS100-43	104	249	118.5	32.1
6-SS100L-44	103	251	165.1	18.7
7-SS100-49	100	-35	162.0	21.9
7-SS100-50	304	-17	100.8	46.2
7-SS100-53	105	293	77.6	32.8
7-SS100-54	100	236	112.2	32.8
7-SS100-55	304	254	77.9	64.1

TABLE A-2 (Cont'd.)

Run	P	T_m	ΔT	h
	Psi	°F	°F	Btu/hr sq ft °F
Stainless Steel Screen -- 10 Mesh				
6-SS10-45	103	234	218.2	7.40
6-SS10L-46	104	217	221.8	5.07
7-SS10-51	106	-66	280.8	6.22
7-SS10-52	305	-53	236.5	10.3
7-SS10-56	103	217	215.6	7.02
7-SS10-57	307	219	174.6	12.8
Laminate T-30LR				
7-LA1/16-11	107	218	215.1	5.04
7-LA2/16-12	108	213	232.3	2.90
7-LA2/16*-13	106	213	233.1	2.90
7-LA3/16-14	104	204	227.4	2.25
7-LA3/16*-15	105	203	222.8	2.61
7-LA4/16-16	106	197	229.7	1.38
7-LA4/16*-17	113	200	236.0	1.35
7-LA3-18	102	206	248.5	1.42
7-LA3*-19	104	205	241.5	1.82
Teflon-TFE				
7-TFE-25	106	286	135.7	28.5
7-TFE-47	104	243	121.6	28.8
7-TFE-48	306	246	123.6	29.9
Special Multi-Layer Test				
$7\text{-}^{MIC2}_{SH}\text{-}28$	102	251	188.5	14.8
$7\text{-}^{MIC2}_{SHP}\text{-}29$	104	256	238.9	9.33

* Material initially compressed to 800 psi

TABLE A-2 (Cont'd.)

Run	P	T_m	ΔT	h
	Psi	^oF	^oF	Btu/hr sq ft ^oF
Special Multi-Layer Test (Cont'd.)				
$7\text{-}^{MIC2}_{MICP}\text{-}30$	104	241	193.5	12.6
$7\text{-}^{MIC2*}_{MICP}\text{-}31$	104	240	193.9	12.8
$7\text{-}^{MIC2}_{SS100}\text{-}32$	103	241	221.6	8.95
$7\text{-}^{MIC2*}_{SS100}\text{-}33$	102	234	198.9	11.1

* Material initially compressed to 800 psi

TABLE A-3

TABULATED EXPERIMENTAL RESULTS

TWO BOLT FLANGE

Run	T_m	ΔT	Q_H	Q_C	Insulation	
	°F	°F	Btu/hr	Btu/hr	Face	Bolts
1-2BT-1	-39	24.3	88.3	91.0	BJ	BJ
1-2BT-2	-28	14.8	86.4	90.5	BJ	BJ
1-2BT-3	333	4.8	83.3	72.6	BJ	BJ
1-2BT-4	287	3.3	85.6	79.5	BJ	BJ
1-2BT-5	304	7.9	78.7	70.3	BJ	BJ
1-2BT-6	9	18.3	84.5	84.9	BJ	BJ
1-2BT-7	277	42.6	252	241	BJ	BJ
1-2BT-8	91	2.0	4.26	5.44	BJ	BJ
1-2BT-9	143	4.5	18.5	18.2	BJ	BJ
1-2BT-10	237	8.0	41.7	35.3	BJ	BJ
1-2BT-11	368	9.8	70.1	54.4	BJ	BJ
2-2BT-1	153	25.1	48.2	45.9	BJ	BJ
2-2BT-2	213	33.9	84.1	79.0	BJ	BJ
2-2BT-3	286	44.1	126	118	BJ	BJ
2-2BT-4	103	13.8	23.1	21.6	BJ	BJ
1-2BT-12	104	12.7	21.8	19.7	BJ	TX
1-2BT-13	151	33.5	47.3	43.8	BJ	TX
1-2BT-14	218	32.5	82.7	77.0	BJ	TX
2-2BT-5	167	39.4	18.2	15.1	CP	BJ
2-2BT-6	260	72.0	35.9	29.0	CP	BJ
2-2BT-7	92	11.8	5.31	4.36	CP	BJ
1-2BT-15	106	57.3	3.76	2.53	CP	TX
1-2BT-16	287	272.1	24.3	15.6	CP	TX

TABLE A-3 (Cont'd.)

Run	T_m °F	ΔT °F	Q_H Btu/hr	Q_C Btu/hr	Insulation Face	Bolts
1-2BT-17	299	209.4	34.5	24.8	CP	TX
1-2BT-18	286	242.5	28.3	19.2	CP	PI
1-2BT-19	287	161.4	37.8	28.1	CP	PI
1-2BT-20	284	199.0	32.7	23.9	CP	TFE
1-2BT-21	305	161.0	42.1	31.9	CP	TFE
1-2BT-22	292	140.9	39.9	30.1	CP	TFE
1-2BT-23	284	51.1	37.3	28.0	MIC2 SH	TFE
1-2BT-24	310	143.0	44.4	33.7	MIC2 SH	TFE
1-2BT-25	309	112.8	47.6	36.4	SI	TFE
2-2BT-8	356	157.9	52.1	39.9	CP	MIC SH
2-2BT-9	328	226.9	38.6	28.1	CP	TX
2-2BT-10	330	146.9	48.8	37.9	CP	SH SS100
2-2BT-11	320	130.7	47.7	36.7	TX	SH SS100
2-2BT-12	154	26.7	19.7	15.4	SS100	SH SS100
2-2BT-13	244	45.2	37.8	30.1	SS100	SH SS100
2-2BT-14	335	61.3	59.9	47.2	SS100	SH SS100

TABLE A-4

TABULATED EXPERIMENTAL RESULTS

FOUR BOLT FLANGE

Run	T_m °F	ΔT °F	Q_H Btu/hr	Q_C Btu/hr	Insulation Face	Insulation Bolts
1-4BT-1	88	5.9	45.5	43.3	BJ	BJ
1-4BT-2	321	9.7	102	89.3	BJ	BJ
1-4BT-3	206	7.8	67.5	59.9	BJ	BJ
1-4BT-4	3	89.4	31.9	31.9	CP	Compression Washer SS100
1-4BT-5	130	113.0	48.5	45.2	CP	Compression Washer SS100
1-4BT-6	252	150.3	74.1	64.4	CP	Compression Washer SS100
1-4BT-7	170	121.1	52.5	46.4	CP	Compression Washer SS100
1-4BT-8	59	46.4	37.0	36.6	SH2 SS100	Compression Washer SS100
1-4BT-9	40	21.0	39.8	39.0	SS100	Compression Washer SS100
1-4BT-10	282	29.1	91.2	79.4	SS100	Compression Washer SS100
1-4BT-11	14	22.7	44.2	41.6	SS100	Compression Washer SS100

APPENDIX B

UNCERTAINTY ANALYSIS

The junction thermal conductance is defined as

$$h = \frac{q}{\Delta T}$$

where q is determined from the product of the thermal conductivity and temperature gradient in the metal test specimen. Since q is evaluated as the product of two terms, the uncertainty as a percentage is given by

$$\frac{\delta(q)}{q} = \left[\left(\frac{\delta k}{k}\right)^2 + \left\{\frac{\delta(dt/dx)}{dt/dx}\right\}^2\right]^{1/2}$$

Some estimate of the uncertainty in the published thermal conductivity values as an estimate a value of 5 percent was selected. For each run a maximum and minimum slope (dt/dx) was read from the plot of specimen temperature versus length. In all cases the slope variation was well within $\pm$ 1°F/inch. From these results a reasonable estimate of the uncertainty in dt/dx is 0.5°F/inch for the low heat flux runs with interstitial materials and perhaps as large as 1-1/2°F/inch for the much greater heat flux tests with the bare junction. All high temperature runs were conducted with water as the coolant and for the interstitial materials the mean temperature varied somewhat with the heat flux. Therefore, the magnitudes of $\delta q/q$, the estimated uncertainty in the calculated heat flux is presented as a function of Q, in Figure B-1. Maximum and minimum possible slopes (dt/dx) were also estimated from the graphs of temperature versus length. The magnitudes

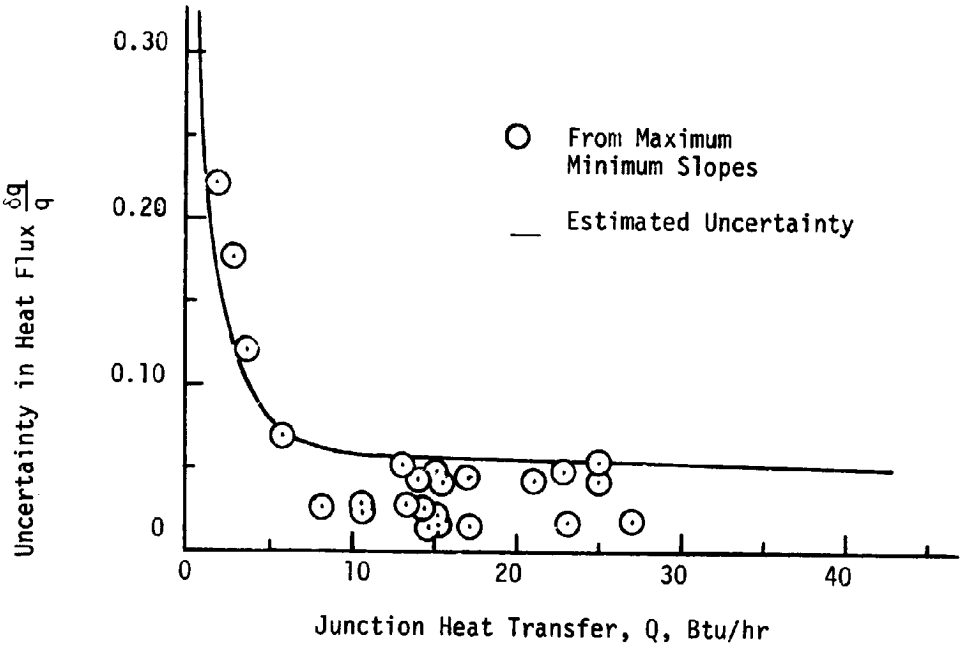

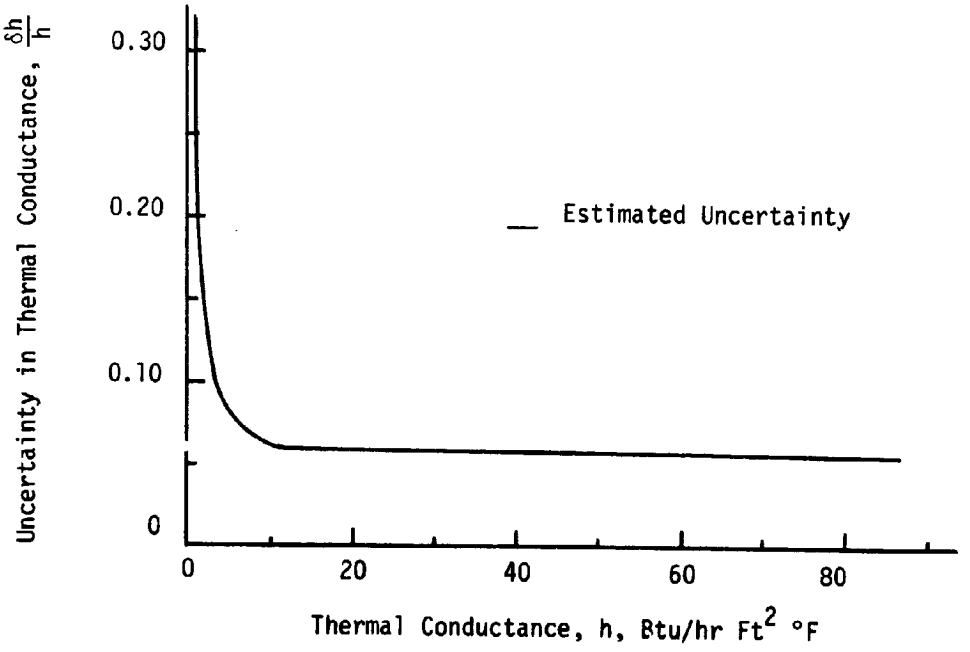

FIGURE B1. Estimated Uncertainty

of $\delta Q/Q$ calculated from these limiting slopes are also plotted in Figure 16. By comparison, the estimated uncertainties in dt/dx and k seem valid. The maximum Q value plotted is 64.1 Btu/hr which corresponds to the 100 mesh stainless steel screen run at 300 psi.

For the interstitial material runs it would be possible to have an error of as much as $4^{\circ}F$ in the value for ΔT, the junction temperature difference. However, from the test results it was estimated that the uncertainty would be between $2^{\circ}F$ and $4^{\circ}F$. For the stainless steel specimens, ΔT was as small as $100^{\circ}F$. Thus the percent uncertainty, $\delta\Delta T/T$, was on the order of 4 percent.

The estimated uncertainties in ΔT and q can be combined to calculate the uncertainty in h,

$$(\delta h/h) = \left[\left(\frac{\delta q}{q}\right)^2 + \left(\frac{\delta \Delta T}{\Delta T}\right)^2\right]^{1/2}$$

Since the magnitude varies with q, hence h, the ratio $\delta h/h$ is presented graphically as a function of h in Figure B-1.

END

DATE

FILMED

OCT 28 1968